VPRBP functions downstream of the androgen receptor and OGT to restrict p53 activation in prostate cancer

Running title: **VPRBP regulates prostate cancer**

Authors

Ninu Poulose[1,2*], Nicholas Forsythe[1], Adam Polonski[3], Gemma Gregg[1], Sarah Maguire[1], Marc Fuchs[1], Sarah Minner[3], Guido Sauter[3], Simon S. McDade[1], Ian G. Mills[1,2,*]

Affiliations

[1]Patrick G Johnston Centre for Cancer Research, Queen's University, Belfast, UK, BT9 7AE.

[2]Nuffield Department of Surgical Sciences, John Radcliffe Hospital, University of Oxford, Oxford, United Kingdom, OX3 9DU.

[3]University Medical Center Hamburg-Eppendorf Department of Pathology, Hamburg, Germany, 20246.

***Co-corresponding Author:** Ian G. Mills, ian.mills@nds.ox.ac.uk

Ninu Poulose, ninu.poulose@nds.ox.ac.uk

Abstract

A comprehensive understanding of androgen receptor (AR) signalling mechanisms during prostate carcinogenesis is instrumental in developing novel therapies. Studies have shown glycosylation as a key androgen regulated process and that O-GlcNAc transferase (OGT), the enzyme that catalyses the covalent addition of UDP-N-acetylglucosamine (UDP-GlcNAc) to serine and threonine residues of proteins, is often up-regulated in prostate cancer (PCa) with its expression correlated with high Gleason score. In this study we have identified an AR and OGT co-regulated factor, VPRBP also known as DCAF1. We show

that VPRBP is regulated by the AR at the transcript level, and stabilized by OGT at the protein level. VPRBP knockdown in PCa cells led to a significant decrease in cell proliferation, p53 stabilization, nucleolar fragmentation and increased p53 recruitment to the chromatin. In human prostate tumor samples, VPRBP protein overexpression correlated with AR amplification, OGT overexpression, early biochemical relapse and poor clinical outcome. Analysis of TCGA datasets found a positive correlation of VPRBP with AR mRNA expression. Furthermore, AR activity gene signature analysis revealed a positive correlation of VPRBP with a subset of AR target genes implying that VPRBP has a preferential regulatory impact on part of the AR regulome. In conclusion, we have shown that VPRBP/DCAF1 promotes PCa cell proliferation by restraining p53 activation under the influence of the AR and OGT as well as uncovered a unique subset of AR activity gene signature that correlates with VPRBP expression with the potential for new avenues for patient stratification and treatment.

Introduction

AR activity plays an important role in the development of localized prostate cancer and also in the sustaining treatment-resistant metastatic disease [1]. AR activation has been shown to enhance flux through hexosamine biosynthetic pathway (HBP) in PCa cell lines [2], which leads to increased bioavailability of UDP-N-acetylglucosamine, a substrate for O-GlcNAcylation as well as N-linked and O-linked glycosylation [3]. O-GlcNAcylation, a highly dynamic and often transient post-translational modification (PTM) is specifically increased in PCa tissues compared to adjacent non-malignant tissues [4]. This PTM is regulated by two enzymes, OGT that catalyses the covalent addition of UDP-N-acetylglucosamine to serine and threonine residues of cytoplasmic, nuclear and mitochondrial proteins, and O-GlcNAcase (OGA) which removes the O-GlcNAc moiety [5]. OGT is considered to be a metabolic rheostat and its

47 expression is elevated in many cancers including PCa, with higher O-GlcNAc levels associated with poor
48 prognosis of patients [6 7]. There is a growing diverse list of proteins which undergo this PTM, including
49 some of the key transcription factors such as c-Myc [8] and p53 [9].
50 A recent ChIP-seq study by Itkonen *et al* has demonstrated that the O-GlcNAc chromatin mark is rapidly
51 lost upon inhibition of OGT activity by a fast-acting inhibitor, OSMI2 [10] in PCa cells. This analysis
52 revealed that the majority of the O-GlcNAc peaks were promoter associated with over 95% overlap with
53 DNase-hypersensitive regions and active chromatin marks. Independent AR ChIP-seq studies from our
54 lab and others have shown that the majority of AR binding sites are distal intergenic and intronic [11].
55 Genome-wide motif co-enrichment, have shown entirely distinct associations between O-GlcNAc and
56 other factors (principally c-Myc and ETS transcription factors), and the AR and other factors (Forkhead
57 family transcription factors such as FOXA1)[11]. Despite these differences, we know that both AR and OGT
58 contribute to PCa progression. To better understand the interplay between OGT and AR in PCa, we
59 analysed these AR and O-GlcNAc ChIP-seq data focusing on promoter proximal sites and identified a
60 small number of overlapping sites and genes. We focussed on VPRBP (Vpr binding protein) also known
61 as DCAF1 (DDB1 and CUL4 Associated Factor 1) which has been implicated as a regulator of cell cycle
62 and cell proliferation[12,13]. VPRBP is the substrate recognition component of cullin 4A-ring E3 ubiquitin
63 ligase (CRL4A) complex as well as separate HECT type EDD/UBR5 E3 ligase [14]. In this study we show
64 that VPRBP is a novel AR target as well as an OGT regulated protein. Knockdown of VPRBP led to a
65 marked reduction in PCa cell proliferation. We go on to show that VPRBP down-regulates p53 stability
66 and activity, and that this is in part by maintaining nucleolar integrity. Tissue microarray studies showed
67 a positive correlation of VPRBP expression with AR/OGT expression and an inverse correlation with PSA
68 recurrence free survival. Furthermore, VPRBP expression in TCGA datasets showed a positive correlation
69 with AR expression and a subset of AR activity gene signatures, and inverse correlation with the p53

70 pathway. We conclude that VPRBP acts as a novel downstream effector of AR and OGT mediated PCa
71 cell proliferation by impairing p53 checkpoint activation.
72
73 **Results**
74 **Identification of VPRBP as a novel AR regulated gene**
75 To identify AR and OGT co-regulated genes, we analysed published AR (GSE28126) and O-GlcNAc
76 (GSE112667) ChIP-seq data. Comparing peak distribution between AR and O-GlcNAc binding sites from
77 these two separate studies (Fig. 1A), indicated that, as previously reported the majority of O-GlcNAc
78 binding sites are promoter proximal, whereas the majority of AR binding sites are intronic or associated
79 with distal inter-genic regions (Fig. 1A). Intersecting LNCaP AR ChIP-seq (R1881 stimulated) binding
80 sites with O-GlcNAc ChIP-seq consensus sites identified only 9 overlapping sites, amongst which a
81 binding site was detected within proximity of *VPRBP* gene (Fig. 1B). VPRBP is of particular interest
82 because it has been shown to be highly expressed in different tumor tissues [15] and is also known to play a
83 pivotal role in cell growth and cell cycle entry in T cells [12]. Moreover, depletion of VPRBP in DU145
84 prostate cancer cells reduced cell proliferation and number of colony forming cells [15]. However the roles
85 of VPRBP in mediating androgen response in PCa or its regulation by OGT or O-GlcNAcylation have not
86 been reported so far.
87 To confirm AR and O-GlcNAc enrichment at the VPRBP site, we performed ChIP-qPCR in LNCaP cells
88 stimulated with 1nM R1881, a synthetic androgen, for 4h and 24h following 72h of androgen deprivation
89 [11111]. We confirmed that as expected androgen stimulation resulted in AR enrichment at a CAMKK2
90 associated site (a known AR target [11]), at both time points (Fig. 1C). By contrast O-GlcNAc enrichment
91 in the promoter of the *PPAT/PAICS* gene [16] was not significantly altered in response to androgen treatment

92 (Fig. 1C and Fig. S1A). Androgen stimulation resulted in increased binding of AR at the VPRBP promoter
93 region at 24h time point (Fig. 1C and Fig. S1A).
94 Quantitative RT-PCR(qRT-PCR) analysis revealed that R1881 stimulated binding of AR to VPRBP
95 promoter correlated with a 2.5 fold increase in VPRBP mRNA expression at 24 h (Fig. 1D), concomitant
96 with a significant increase in VPRBP protein levels 24 and 48 hours (Fig. 1E and Fig. S1B). OGT and O-
97 GlcNAcylation levels also showed significant increases following R1881 stimulation at the later time
98 points (Fig. 1E and Fig.S1B). CAMKK2 and UAP1 expression levels were used as positive controls [11].
99 Since R1881 is a synthetic androgen, we also tested the effect of endogenous androgen,
100 dihydrotesteosterone (DHT). Similarly to R1881, stimulation of LNCaP cells by DHT for 24h also
101 increased VPRBP mRNA and protein expression (Fig. S1C and Fig. S1D).

102 **OGT is required for VPRBP stability**

103 To determine if OGT is required for VPRBP expression, we performed OGT knockdown using siRNA.
104 This revealed that there was no significant change in basal VPRBP mRNA levels in OGT siRNA
105 transfected cells compared to scrambled control (Fig. 2A). Interestingly, OGT knockdown reduced both
106 basal (Fig. 2B) and androgen-induced (Fig. 2C) VPRBP expression. OGT siRNA transfection resulted in
107 >90% reduction in basal OGT protein expression and >80% reduction in total O-GlcNAc levels with both
108 siRNAs (Fig. S2A). There was ~57% reduction in VPRBP protein expression with OGTsiRNA1 and
109 ~54% with OGT siRNA2 5d post transfection (Fig. S2A). Overall, these results suggest a possible dual
110 regulation of VPRBP, whereby VPRBP is induced at the mRNA level by AR and is stabilised post-
111 translationally by OGT activity.
112 O-GlcNAcylation has been shown to affect the stability of proteins like p53 [9], c-Myc [2] and EZH2 [17].
113 Therefore we performed immunoprecipitation (IP) to test the O-GlcNAcylation status of VPRBP. IP
114 indicates that VPRBP is an O-GlcNAcylated protein (Fig. 2D). To further confirm if O-GlcNAcylation is

115 necessary for the stability of VPRBP, we treated the cells with inhibitors of OGT activity, OSMI2 and
116 OSMI3 [18]. We found that treatment for 24h decreased VPRBP expression at the protein level by ~73% for
117 40 μM OSMI2 and ~62% for 10 μM OSMI3 (Fig. 2E and Fig. S2B). OSMI treatment reduced overall O-
118 GlcNAcylation levels with a compensatory up-regulation of OGT expression (Fig. 2E and Fig. SB). There
119 was no significant change in VPRBP expression at the transcript level with OSMI3 treatment, although
120 OSMI2 exhibited a small reduction of VPRBP transcripts (Fig. S2C).

121 **VPRBP down-regulation stabilizes p53 and inhibits LNCaP cell proliferation**

122 Having identified VPRBP as an AR and OGT target, we went on to determine the functional effect of
123 VPRBP knockdown in LNCaP cells. Knockdown with VPRBP siRNA resulted in ~75% reduction in
124 VPRBP mRNA expression (Fig. 3A). A ~57% reduction in cell number was observed with VPRBP
125 siRNAs when cells were grown in complete growth media containing androgens whereas androgen
126 deprivation on its own resulted ~38% in a reduction in cell numbers (Fig. 3B). Furthermore, chemical
127 inhibition by B32B3, a potent and selective inhibitor of VPRBP kinase activity [15], led to ~64% decrease
128 in LNCaP cell proliferation at 5μM concentration (Fig. S3A). The combination of B32B3 and OGT
129 inhibitors did not show significant decreases in cell numbers compared to B32B3 alone (Fig. S3A).

130 VPRBP knockdown in LNCaP led to a substantial increase in p53 protein expression and its downstream
131 targets cyclin dependent kinase inhibitor p21[19] and Mdm2[20] (Mouse double minute 2 homolog), (Fig. 3C
132 and Fig. S3B). Consequently we observed a drastic reduction in cell cycle markers like phospho CDK2
133 Thr160 [21] , Cyclin B1 [22] , polo-like kinase1 (PLK1) [23], phospho-histone H3 ser10 [24] and Phospho-PP1α
134 Thr320 [25] (Fig. 3C and Fig. S3B) following VPRBP knockdown. In summary, VPRBP tightly control cell
135 proliferation mainly by regulating the expression of p53. It is interesting to note that whereas VPRBP
136 knockdown led to p53 stabilization, the reduction in VPRBP levels by OGT knockdown did not translate

137 to similar effects (Fig. 2B). This is likely because p53 itself is an O-GlcNAcylated protein whose stability
138 is enhanced with O-GlcNAcylation at Ser 149 position [9].
139 In order to determine if the growth inhibitory effects of VPRBP knockdown were primarily mediated
140 through p53, we performed VPRBP knockdown in the VCaP, a cell-line expressing mutant p53. VPRBP
141 knockdown in VCaP failed to cause significant changes in cell numbers (Fig. 3D) and cell cycle markers
142 (Fig. 3E), indicating a crucial role for p53 in mediating VPRBP effects in PCa. However, similarly to
143 LNCaP, VPRBP knockdown in VCaP cells reduced c-Myc levels (Fig. 3E). Together, these results suggest
144 that the growth inhibitory effects of VPRBP knockdown are primarily mediated through p53 stabilization
145 and activation.
146 Furthermore, we observed a reduction in p53 protein (Fig. S4A) and mRNA expression (Fig. S4B) in
147 LNCaP cells following R1881 stimulation, and a corresponding decrease in p53 enrichment at p21
148 (CDKN1A) promoter by ChIP-qPCR (Fig. S4C) suggesting that pro-proliferative effects of androgens
149 may partly be mediated by factors that down-regulate p53. However VPRBP gene itself does not appear
150 to be p53 regulated, since there was no significant enrichment by ChIP-qPCR (Fig. S4D) and no binding
151 sites were identified within its promoter region from p53 ChIP-seq in nutlin-3a treated LNCaP cells (Fig.
152 S4E). Analysis of a novel p53-knockout LNCaP cell-line showed higher basal levels of VPRBP. By
153 contrast treating LNCaP cells with a p53 stabilizer, nutlin-3a, led to a decrease in VPRBP (Fig. S4F and
154 Fig. S4G). Consequently a reciprocal feedback relationship between VPRBP and p53 expression seems
155 to exist within these cells.
156
157 **p53 ChIP-seq reveals increased p53 recruitment to the chromatin following VPRBP knockdown**
158 To further establish whether VPRBP was influencing p53 activity, we performed p53 ChIP-seq in LNCaP
159 cells following siRNA knockdown with VPRBP, OGT and non-targeting siRNAs along with nutlin-3a

160 treated samples. Canonical p53 target gene p21 (CDKN1A) was used as a positive control to validate ChIP
161 efficiency by ChIP-qPCR (Fig. 4A). This is the first report on p53 ChIP-seq in a prostate cancer cell line.
162 Overall, there were fewer p53 peaks in LNCaP (Fig. 4B) than reported in other cell types [26,27], suggesting
163 fundamental differences in p53 transcriptional landscape amongst these cells. ChIP-seq in nutlin-3a
164 treated LNCaP cells returned 582 peaks, the majority of which (>80%) overlapped with nutlin-3a p53
165 ChIP-seq binding sites in other cell lines confirming they are bona fide p53 binding sites (Fig. 4C and Fig.
166 S5A). By contrast VPRBP knockdown led to a ~4.7 fold increase in the number of p53 genomic binding
167 sites compared to the scrambled control (Fig. 4B). There were 1387 consensus p53 binding sites between
168 the two VPRBP knockdown samples (si1 and si2) representing a site overlap between these conditions of
169 ~85%. The vast majority (~95%) of LNCaP nutlin-3a p53 ChIP-seq sites were present within this
170 consensus suggesting that VPRBP knockdown expanded the number of p53 accessible sites (Fig. 4D).
171 Importantly the majority of sites in VPRBP knockdown overlapped with nutlin-3a MCF7 p53 ChIP-seq
172 peaks (Fig. 4E). The majority of OGT si1 and OGT si2 sites overlapped, so was there a significant overlap
173 of OGT si consensus sites with VPRBP si consensus sites and scr si sites (Fig. S5B).
174 Assessing the distribution of p53 peaks revealed that the majority were present in distal intergenic regions
175 (45-54%), with around 6% binding events in proximal promoters (Fig. S5C), resembling the AR binding
176 pattern. The VPRBP si p53 ChIP-seq peaks showed ~53% overlap with H2K27Ac peaks and ~0.7%
177 overlap with H3K27me3 peaks indicating majority of the binding sites are present at sites of
178 transcriptional activity which are not accessible to p53 when VPRBP is expressed (Fig. S5D). The genes
179 within 10kb of p53 sites in the VPRBP knockdown condition were identified (Supplementary file 2).
180 These included established p53 target genes such as CDKN1A and MDM2. Motif enrichment analysis on
181 the p53 sites in the knockdown condition showed an over-representation of TP53, TP73 and TP63 binding

182 motifs (Fig. S5E). Together these suggest that VPRBP may restrain p53 activity by occluding chromatin
183 and that VPRBP knockdown expands the gene regulatory network affected by increased p53 expression.

184 **VPRBP knockdown induces nucleolar stress in LNCaP cells**

185 A comparison of VPRBP interactome (147 proteins) obtained from BioGRID database [28] (supplementary
186 file 3) with nucleolar proteome (1314 proteins) of human cells derived from the Cell Atlas [29] showed that
187 ~14 % of VPRBP interactors also show nucleolar localization (Fig. 4F). VPRBP is also reported to be
188 involved in 40S ribosomal subunit biogenesis along with other CRL4 E3 ubiquitin ligase and COP9
189 signalosome components in a genome wide RNAi screen study [30]. Hence we hypothesised that VPRBP
190 knockdown may enhance p53 stability and diminish ribosome biogenesis by destabilising the nucleolus.
191 Our immunofluorescence studies showed both cytoplasmic and nucleolar localization of VPRBP (Fig.
192 4G) as reported previously [31] [32]. Reduction in the number of nucleoli and/or disintegration of nucleolar
193 structures are some of the characteristic features of nucleolar stress [33]. We found a marked change in
194 staining pattern of nucleolar protein fibrillarin following VPRBP siRNA knockdown, indicative of
195 nucleolar stress (Fig. 4G). Fibrillarin showed exclusive nucleolar localization with a redistribution to small
196 nucleoplasmic entities in the VPRBP knockdown cells, similar to previously described with actinomycin
197 D treatment [34]. A significant (~25%) reduction in fibrillarin and 40S ribosomal protein S8 (RPS8)
198 expression, was observed with VPRBP siRNA2 (Fig. S6A and Fig. S6B.) This suggests that VPRBP
199 knockdown contributes to p53 stabilization by imposing nucleolar stress.

200 **VPRBP expression correlates with AR expression in clinical samples and is prognostic**

201 To further understand the prognostic potential of VPRBP in PCa, we analysed its expression in tissue
202 microarrays (TMA) by IHC. The representative images of negative, low, intermediate and high staining
203 of VPRBP are shown in Fig. S6C. We assessed its correlation with PCa pathology, and with the AR and
204 OGT. We observed that 46% of all tumors stained strongly for VPRBP expression with a statistically

205 significant increase in protein levels with tumor stage and quantitative Gleason grade (Supplementary
206 Table 6). Although there were few Gleason score 7 tumors with tertiary Gleason pattern 5 (a powerful
207 predictor of biochemical relapse [35]), all of them were VPRBP-positive. A higher VPRBP staining was
208 observed in cases with positive surgical margins (Supplementary Table 6). However, there were no
209 significant differences in VPRBP expression between patients with no regional lymph node metastasis
210 (N0) and patients with metastasis (N+). Significant correlations were also not seen between VPRBP
211 expression and pre-operative PSA levels (Supplementary Table 6). To determine whether VPRBP
212 expression associated with poor prognosis disease, we evaluated its expression versus post-operative
213 biochemical (PSA) recurrence-free survival. We observed a statistically significant reduction in PSA
214 recurrence-free survival in patients with any VPRBP expression compared to those who were negative
215 (Fig. S6D). We went on to assess the co-expression of VPRBP with AR or OGT in the TMA. For both,
216 we observed a statistically significant positive correlation in staining which suggests that the expression
217 and activity of these proteins may be relevant in subsets of patients (Fig. 5A and Fig. 5B). Furthermore
218 VPRBP positive/AR high groups exhibited a statistically significant reduction in PSA recurrence-free
219 survival when compared to VPRBP negative/AR low groups (p=0.0019); and so did VPRBP
220 positive/OGT high groups compared to VPRBP negative/OGT negative (p=0.0013) (Fig. 5C and Fig. 5D).
221 We next sought to determine whether VPRBP transcript expression in clinical samples is associated with
222 activity gene signatures reflecting AR activity. First we compared the VPRBP mRNA expression in the
223 TCGA datasets and found a positive correlation with AR mRNA expression (Fig. 5E). There have been
224 multiple studies reporting AR activity gene signatures. In order to identify the subset of AR activity gene
225 signatures which are highly expressed in VPRBP high tumors, we combined AR activity gene signatures
226 from Dorothea AR regulon, KEGG prostate cancer pathway and an additional 8 gene sets from the
227 Molecular Signatures Database (MSigDB) and clustered them on VPRBP high and low expression

228 quartiles as a heatmap (Combined AR gene list in supplementary file 4) (Fig. S7). These gene sets included
229 Nelson androgen stimulated down (17 genes), Nelson androgen stimulated up (83 genes)[36], PID AR non-
230 genomic (31 genes), PID AR pathway (61 genes), PID AR TF (53 genes), TAKAYAMA bound by AR
231 (10 genes)[37], Wang response up (28 genes) [38] and Wiki pathway androgen pathway signaling (91 genes).
232 Combined, these studies have attributed the expression of 467 genes to AR activity. Since it is not clear
233 which may be most relevant in a given patient group we assessed all of them relative to VPRBP quartile
234 expression in the TCGA Prostate Cancer dataset (Fig.S7). 139 of these 467 genes positively correlated
235 with VPRBP expression and 92 negatively correlated with VPRBP expression (Supplementary file 5).
236 The association between VPRBP expression quartiles and the 139 genes is illustrated in a box plot and is
237 statistically significant between the quartiles Fig. 6F. Importantly the 139 genes most significantly
238 associated with AR responsive pathways but did not include some canonical AR targets such KLK2 and
239 KLK3. In order to further refine this association, we generated co-expression tables for the TCGA dataset
240 ranking all genes that were co-expressed with VPRBP according to a Spearman rank correlation
241 coefficient. We also did this for two other datasets, SU2C/PCF Dream Team, Cell 2015 and MSKCC,
242 Cancer Cell, 2010 from cBioPortal. 48 genes amongst the 139 genes identified were significantly co-
243 expressed with VPRBP (Spearman rank coefficient threshold >0.4) in all the three studies (Supplementary
244 file 5). This represents putative VPRBP-dependent AR regulome which will form the basis for future
245 mechanistic studies on the interplay between VPRBP and AR activity. Next we looked at the p53 activity
246 signatures and found an inverse correlation of VPRBP expression with HALLMARK_P53_pathway [39]
247 (Fig. 6G). We also evaluated VPRBP expression versus a second gene signature reflecting p53 activity
248 derived from perturbation experiments (progeny) [40] in the Taylor datasets. This also showed a statistically
249 significant inverse correlation (Fig. 6H). Together these studies underscore the significance of VPRBP in
250 promoting PCa growth and progression.

251

252 **Discussion**

253 Our previous studies attributed the impact of O-GlcNAc/OGT on PCa cells to effects on c-Myc stability
254 [2], and based on ChIP-seq data, to the over-representation of c-Myc at O-GlcNAc binding sites in the
255 genome [10]. Though the majority of O-GlcNAc peaks in the genome are promoter proximal and associated
256 with histone marks indicative of active transcription [10], the majority of AR sites are distal intergenic or
257 intronic. However, we observed that a small number of AR binding sites overlapped with O-GlcNAc sites
258 on chromatin and hypothesised that these might help us to identify factors that were co-regulated by the
259 AR and OGT. The potential biological significance of these sites is underscored by the fact that in our
260 case they have led us to uncover VPRBP as a novel AR and OGT target.

261 VPRBP was initially identified as a protein targeted by HIV-1 viral protein R (Vpr) to initiate host cell
262 response leading to cell cycle arrest at G2/M by hijacking the CUL4A E3 ubiquitin ligase machinery [31 41].
263 This implies that VPRBP can in some settings support cell cycle progression and indeed we know this to
264 be the case from previous studies [42]. We show that VPRBP is transcribed in response to androgen treatment
265 (Fig. 1D) and that its protein stability is dependent on OGT (Fig. 2B and Fig. 2E). We went on to show
266 that knockdown of VPRBP by siRNA led to significant decrease in LNCaP proliferation accompanied by
267 stabilization of tumor suppressor p53 (Fig. 3C). Guo *et al* [12] demonstrated similar stabilization of p53 in
268 T cells following VPRBP deletion suggesting its requirement in Mdm2-mediated p53 poly-ubiquitination
269 [12]. They further show that for T cell proliferation to occur, VPRBP promotes cell cycle entry by restraining
270 p53 activation whilst a VPRBP-dependent, p53-independent programme possibly involving c-Myc
271 dictates cell growth in naive T cells after T-cell receptor (TCR) activation. [12]. One can draw some
272 similarities between T cells progressing from quiescence to proliferation and prostate cancer cells during
273 androgen stimulation. During TCR activation, cells undergo drastic metabolic changes with increased

274 glucose and glutamine uptake, and a concomitant increase in O-GlcNAcylation [43]. Comparably, androgen
275 stimulation of PCa cells increased glucose uptake and anabolic synthesis of glutamine [11]. Androgen
276 stimulated cells also displayed higher HBP pathway enzymes and protein O-GlcNAcylation levels (Fig.
277 1E). Interestingly, VPRBP is upregulated upon TCR activation in T cells as well as with AR activation in
278 PCa cells. Collectively our data suggest that the similar dependencies on both VPRBP and OGT for cell
279 proliferation exist for both PCa cells and T cells.
280 Other than stabilization, the regulation of p53 transcriptional activity by VPRBP has been previously
281 described by Kim *et al* [44] to occur at the chromatin level. In this study they showed that VPRBP is recruited
282 to target promoters by p53 to attenuate p53 dependent transcription by selectively binding to the
283 unacetylated histone H3 tails in the absence of any stress stimuli rendering it inaccessible to Histone acetyl
284 transferases. They also showed that VPRBP knockdown led to activation of p53 target genes, so did its
285 phosphorylation at ser-895 by DNA-activated protein kinase (DNA-PK). A follow up study by the same
286 group further identified a novel intrinsic kinase activity of this protein towards histone H2A on threonine
287 120 which favours its localization to tumor suppressor genes and chromatin silencing [15]. In our study we
288 have shown that VPRBP knockdown significantly enhances the recruitment of p53 to chromatin as
289 assessed by a significant increase in genome-wide p53 binding sites. Collectively, these suggest that
290 VPRBP is a multi-stage inhibitor of p53 activation, impacting on both chromatin binding and p53 stability
291 and expression. This impact may however be most profound in cells expressing wild-type p53 since a
292 mutant p53 cell-line, VCaP, did not show significant reductions in p53 levels with VPRBP knockdown
293 (Fig. 3E). We also tested the feedback effects of p53 activation on VPRBP expression and have found that
294 stabilising p53 pharmacologically with nutlin-3a diminishes VPRBP stability and knocking out p53
295 enhances it (Fig. S4F). We believe this is predominantly a post-translational/protein turnover effect since
296 there are no significant changes in transcript levels (Fig. S4G) and no evidence of p53 binding to the

297 VPRBP promoter (Figure S4E). All the above studies suggest a reciprocal relation between p53 and
298 VPRBP in PCa cells.
299 We have also shown previously that inhibiting guanine nucleotide biosynthesis disrupts nucleolar function
300 leading to p53 stabilization and c-Myc downregulation [16]. In that study we reported that inhibiting
301 IMPDH2 with a drug, mycophenolic acid, led to p53 stabilisation by depleting cellular GTP levels,
302 promoting degradation of nucleolar proteins such as GNL3 and thereby inducing nucleolar stress [16].
303 Interestingly mycophenolic acid was developed and used initially to restrict T and B cell proliferation for
304 the purposes of enhancing graft take in patients undergoing renal transplant surgery [45]. This further
305 reinforces the idea that there are significant commonalities in the biological processes that support immune
306 activation mediated T-cell proliferation and PCa cell proliferation. Since VPRBP was previously shown
307 to sustain 40S ribosome subunit biogenesis by supporting nucleolar integrity [30], we were led to test how
308 targeting VPRBP might affect this compartment. Imaging of nucleolar marker, fibrillarin revealed marked
309 changes in nucleolar staining indicative of nucleolar stress (Fig. 4G). A recent study by Han *et al* revealed
310 a critical role for VPRBP in rRNA processing and ribosome biogenesis by regulating a previously
311 unknown substrate, the ribosome assembly factor PWP1 [13]. Interestingly, VPRBP loss leads to
312 accumulation of free ribosomal protein L11 (RPL11), resulting in L11-MDM2 association and p53
313 activation. Together, we conclude that VPRBP restricts p53 activation in part by maintaining nucleolar
314 integrity.
315 By examining the VPRBP protein expression in tissue from a highly annotated PCa patient cohort, we
316 established that expression increases significantly with stage and grade and furthermore correlates
317 positively with high expression of the AR and OGT. Future studies will also need to further dissect the
318 functional impact of VPRBP in a range of other mutational backgrounds include RB-loss, PTEN-loss and
319 p53 point mutation. In conclusion VPRBP represents the first AR and OGT co-regulated protein to

320 promote prostate cancer cell proliferation by limiting p53 activation and as such may be an early
321 determinant of prostate cancer progression (Findings summarized in Fig.6). Based on our studies and
322 previous studies on T cell proliferation and activation we believe that it works hand-in-glove with c-Myc
323 to support proliferation. It would be relevant to include VPRBP in patient stratification for treatment
324 optimization in men with PCa.

325 **Materials and Methods**

326 **Reagents and consumables**

327 Synthetic androgen, R1881 and dihydrotestosterone were obtained from Sigma-Aldrich. OGT inhibitors,
328 OSMI2 and OSMI3 were kindly provided by Professor Suzanne Walker (Harvard Medical School,
329 Boston, MA, USA). Formaldehyde 16% (F017/3) was purchased from TAAB laboratory. iDeal ChIP-seq
330 Kit for Transcription Factors (C01010170) was obtained from Diagenode. B32B3 (SML1419) was
331 purchased from Sigma-Aldrich. Antibody details are provided in supplementary table 1. Lipofectamine
332 RNAiMAX Transfection Reagent (13778075) was obtained from ThermoFisher scientific. Protein A
333 sepharose beads (ab193256) and protein G sepharose beads (ab193259) were from abcam.

334 **Cell lines**

335 LNCaP cells were purchased from ATCC and cultured in Roswell Park Memorial Institute media (RPMI)
336 containing 10% fetal bovine serum and 1% pencillin-streptomycin in a humidified incubator at 37^0C and
337 5% CO_2. VCaP cells were obtained from ATCC and cultured in Dulbecco's Modified Eagle Media
338 (DMEM) containing 10% fetal bovine serum and 1% pencillin-streptomycin in a humidified incubator at
339 37^0C and 5% CO_2. TP53 CRISPR knockout LNCaP cells were provided by Dr.Simon McDade (Queen's
340 University, Belfast, UK; supplementary materials and methods)

341 **Chromatin immunopreciptation (ChIP) assays**

342 ChIP assays were carried out as per manufacturer's instructions (Details in supplementary materials and
343 methods).

344 **Real time qPCR**

345 The cells were lysed in qiazol and RNA isolated using Qiagen miRNeasy mini kit (Cat # 217004).
346 Transcriptor first strand cDNA synthesis kit (Cat # 04897030001, Roche Life science) was used for cDNA
347 preparation. SYBR Green 1 Master (Cat# 4887352001, Roche Life science) was used to compare gene
348 expression changes in VPRBP, OGT, CAMKK2, UAP1, COPS3, p53 and p21 by realtime qPCR in Roche
349 LightCycler® 480 Instrument II. Human large ribosomal protein (RPLPO) was used as the internal
350 control. Primers for realtime PCR were purchased from either Sigma (KiCqStart predesigned) or from
351 Eurofins genomics. The primer details are provided in supplementary table 3 and 4 respectively.

352 **siRNA transfection**

353 LNCaP cells were seeded on to 6 well plates for siRNA knockdown. Forward transfection was performed
354 the following day using Lipofectamine RNAiMAX Transfection Reagent in OPTI-MEM with 30 pmol of
355 siRNA/well according to the manufacturer's instructions. After overnight incubation, media was changed
356 to RPMI with 10% FBS and antibiotics. Two individual siRNAs were used against each target of interest.
357 The siRNAs used were OGT si1, OGT si2, DCAF1 si1, DCAF1 si2, and Silencer™ Select Negative
358 Control No.1 siRNA (Details are provided in supplementary table 5). For studies involving androgen
359 treatment, media was changed to androgen deprived charcoal-treated media for 3 days prior to stimulation
360 with 1 nM R1881 for 24h. The cells were lysed after given number of days post transfection for analysis
361 by western blot or real time PCR.

362 **Western blot analysis**.

363 The cells were lysed in RIPA buffer (Sigma) containing protease inhibitor cocktail (Roche) and
364 PhosSTOP™ (Sigma); protein concentration estimated with Bradford reagent (Biorad) and 30 µg of lysate

365 subjected to electrophoresis using precast 4–12% NuPage mini-gels (Life Technologies). The resolved
366 proteins were then transferred to PVDF membrane, blocked with 5% nonfat dry milk and probed with
367 respective primary antibodies overnight at 4^0C. After 3 washes, the blots were probed with HRP-
368 conjugated secondary antibodies and immunoreactivity detected by enhanced chemiluminescence in
369 Syngene G box.

370 **Immunoprecipitation**

371 Briefly, LNCaP cells were lysed in IP lysis buffer (10mM Tris-Cl pH7.5, 140mM NaCl, 1mM EDTA, 1%
372 Triton X-100, 0.1% sodium deoxycholate, 0.1% SDS). Lysates were precleared with protein A sepharose
373 beads for 1h at 4^0C in a rotator. Immunoprecipitation (IP) was carried out with protein A sepharose beads
374 using 1mg lysate and 1 µg VPRBP antibody. Lysate was incubated with VPRBP or IgG negative control
375 antibody for 3h at 4^0C in a rotator followed by overnight incubation with 40µl of washed protein A
376 sepharose beads. The beads were briefly pelleted and washed thrice in IP wash buffer (10mM Tris-Cl
377 pH7.5, 150mM NaCl, 0.5% Triton X-100). The proteins were eluted by heating in 20 µl laemelli buffer
378 at 95^0C for 5min.

379 **Cell counts**

380 Cell counting of siRNA transfected cells in 12 well plates was performed 5d post transfection. Cells were
381 trypsinized and changes in cell number assessed by cell counting in Countess II Lifetechnologies.

382 **Immunoflourescence**

383 LNCaP cells were seeded on to glass coverslips in a 12 well plate. After reaching 70-80% confluence,
384 cells were transfected with scrambled or VPRBP siRNA. After 3 days, cells were fixed with 4%
385 paraformaldehyde in BSA for 10 min followed by three washes in PBS for 5 min each. The fixed cells
386 were then lysed in 0.1% TX100 in PBS for 10 min and blocked in blocking buffer (5% goat
387 serum/1%BSA/0.1%TX100 in PBS) for 1h. The cells were then incubated in primary antibodies against

388 VPRBP (1:80) and fibrillarin (1:100) for 2h at RT followed by Alexa flour 594 Goat anti mouse
389 (Invitrogen, Cat # A11020) or Alexa flour 488 Goat Anti R (Invitrogen, Cat # A11070) secondary
390 antibodies. Coverslips were mounted on to glass slides using Vectashield with DAPI.
391 Patients**,** immunohistochemistry and analysis of TCGA and other datasets can be found in supplementary
392 materials and methods

393 **Statistical analysis**

394 Statistical analyses for studies in LNCaP and VCaP cells were done using either student's t-test or one
395 way ANOVA with Tukey's posthoc analysis, as mentioned in the figure legends. For IHC, statistical
396 calculations were performed using JMP 12® software (SAS Institute Inc., NC, USA). Contingency tables
397 were calculated with the chi²-test. Survival curves were calculated by the Kaplan-Meier method and
398 compared with the Log rank test.

399 **Acknowledgments**

400 This research was supported by the Norwegian Research Council (230559). IGM is also supported by the
401 Prostate Cancer UK/ Movember Centre of Excellence (CEO13_2–004) and the John Black Charitable
402 Foundation. Authors would like to acknowledge Genomic Core Technology Units, Queens University
403 Belfast for the assistance with ChIP-seq studies.

404 **Author contributions:** NP designed and performed the experiments, prepared samples for sequencing,
405 analyzed the data and wrote the manuscript. AP, GS and Sarah Minner performed IHC and evaluated
406 expression in prostate tumours. NF performed analysis on TCGA, Taylor and other datasets from
407 MSigDB. GG generated p53 knockout LNCaP cells under the supervision of SMcD. SMcD reviewed and
408 edited the manuscript. MF performed the fragment analysis for ChIP-seq samples and conducted the
409 Illumina NextSeq™ 500 sequencing run. Sarah Maguire generated the fastq files, bam files and bed files.
410 IGM supervised the study, reviewed and edited the manuscript.

411 **Competing interests:** The authors declare no competing interests.

412

413 **References**

414

415 1 Feng, Q. & He, B. Androgen Receptor Signaling in the Development of Castration-Resistant
416 Prostate Cancer. *Front Oncol* **9**, 858, doi:10.3389/fonc.2019.00858 (2019).
417 2 Itkonen, H. M. *et al.* O-GlcNAc transferase integrates metabolic pathways to regulate the
418 stability of c-MYC in human prostate cancer cells. *Cancer Res* **73**, 5277-5287,
419 doi:10.1158/0008-5472.CAN-13-0549 (2013).
420 3 Akella, N. M., Ciraku, L. & Reginato, M. J. Fueling the fire: emerging role of the hexosamine
421 biosynthetic pathway in cancer. *BMC Biol* **17**, 52, doi:10.1186/s12915-019-0671-3 (2019).
422 4 Gu, Y. *et al.* O-GlcNAcylation is increased in prostate cancer tissues and enhances malignancy
423 of prostate cancer cells. *Mol Med Rep* **10**, 897-904, doi:10.3892/mmr.2014.2269 (2014).
424 5 Bond, M. R. & Hanover, J. A. A little sugar goes a long way: the cell biology of O-GlcNAc. *J*
425 *Cell Biol* **208**, 869-880, doi:10.1083/jcb.201501101 (2015).
426 6 Fardini, Y., Dehennaut, V., Lefebvre, T. & Issad, T. O-GlcNAcylation: A New Cancer
427 Hallmark? *Front Endocrinol (Lausanne)* **4**, 99, doi:10.3389/fendo.2013.00099 (2013).
428 7 Kamigaito, T. *et al.* Overexpression of O-GlcNAc by prostate cancer cells is significantly
429 associated with poor prognosis of patients. *Prostate Cancer Prostatic Dis* **17**, 18-22,
430 doi:10.1038/pcan.2013.56 (2014).
431 8 Yang, X. & Qian, K. Protein O-GlcNAcylation: emerging mechanisms and functions. *Nat Rev*
432 *Mol Cell Biol* **18**, 452-465, doi:10.1038/nrm.2017.22 (2017).
433 9 Yang, W. H. *et al.* Modification of p53 with O-linked N-acetylglucosamine regulates p53
434 activity and stability. *Nat Cell Biol* **8**, 1074-1083, doi:10.1038/ncb1470 (2006).
435 10 Itkonen, H. M. *et al.* High OGT activity is essential for MYC-driven proliferation of prostate
436 cancer cells. *Theranostics* **9**, 2183-2197, doi:10.7150/thno.30834 (2019).
437 11 Massie, C. E. *et al.* The androgen receptor fuels prostate cancer by regulating central metabolism
438 and biosynthesis. *EMBO J* **30**, 2719-2733, doi:10.1038/emboj.2011.158 (2011).
439 12 Guo, Z. *et al.* DCAF1 controls T-cell function via p53-dependent and -independent mechanisms.
440 *Nat Commun* **7**, 10307, doi:10.1038/ncomms10307 (2016).
441 13 Han, X. R. *et al.* CRL4(DCAF1/VprBP) E3 ubiquitin ligase controls ribosome biogenesis, cell
442 proliferation, and development. *Sci Adv* **6**, doi:10.1126/sciadv.abd6078 (2020).
443 14 Schabla, N. M., Mondal, K. & Swanson, P. C. DCAF1 (VprBP): emerging physiological roles
444 for a unique dual-service E3 ubiquitin ligase substrate receptor. *J Mol Cell Biol* **11**, 725-735,
445 doi:10.1093/jmcb/mjy085 (2019).
446 15 Kim, K. *et al.* VprBP has intrinsic kinase activity targeting histone H2A and represses gene
447 transcription. *Mol Cell* **52**, 459-467, doi:10.1016/j.molcel.2013.09.017 (2013).
448 16 Barfeld, S. J. *et al.* Myc-dependent purine biosynthesis affects nucleolar stress and therapy
449 response in prostate cancer. *Oncotarget* **6**, 12587-12602, doi:10.18632/oncotarget.3494 (2015).
450 17 Lo, P. W. *et al.* O-GlcNAcylation regulates the stability and enzymatic activity of the histone
451 methyltransferase EZH2. *Proc Natl Acad Sci U S A* **115**, 7302-7307,
452 doi:10.1073/pnas.1801850115 (2018).

453 18 Martin, S. E. S. *et al.* Structure-Based Evolution of Low Nanomolar O-GlcNAc Transferase
454 Inhibitors. *J Am Chem Soc* **140**, 13542-13545, doi:10.1021/jacs.8b07328 (2018).
455 19 Karimian, A., Ahmadi, Y. & Yousefi, B. Multiple functions of p21 in cell cycle, apoptosis and
456 transcriptional regulation after DNA damage. *DNA Repair (Amst)* **42**, 63-71,
457 doi:10.1016/j.dnarep.2016.04.008 (2016).
458 20 Barak, Y., Juven, T., Haffner, R. & Oren, M. mdm2 expression is induced by wild type p53
459 activity. *EMBO J* **12**, 461-468 (1993).
460 21 Gu, Y., Rosenblatt, J. & Morgan, D. O. Cell cycle regulation of CDK2 activity by
461 phosphorylation of Thr160 and Tyr15. *EMBO J* **11**, 3995-4005 (1992).
462 22 Lindqvist, A., van Zon, W., Karlsson Rosenthal, C. & Wolthuis, R. M. Cyclin B1-Cdk1
463 activation continues after centrosome separation to control mitotic progression. *PLoS Biol* **5**,
464 e123, doi:10.1371/journal.pbio.0050123 (2007).
465 23 Gheghiani, L., Loew, D., Lombard, B., Mansfeld, J. & Gavet, O. PLK1 Activation in Late G2
466 Sets Up Commitment to Mitosis. *Cell Rep* **19**, 2060-2073, doi:10.1016/j.celrep.2017.05.031
467 (2017).
468 24 Van Hooser, A., Goodrich, D. W., Allis, C. D., Brinkley, B. R. & Mancini, M. A. Histone H3
469 phosphorylation is required for the initiation, but not maintenance, of mammalian chromosome
470 condensation. *J Cell Sci* **111 (Pt 23)**, 3497-3506 (1998).
471 25 Berndt, N., Dohadwala, M. & Liu, C. W. Constitutively active protein phosphatase 1alpha causes
472 Rb-dependent G1 arrest in human cancer cells. *Curr Biol* **7**, 375-386, doi:10.1016/s0960-
473 9822(06)00185-0 (1997).
474 26 Andrysik, Z. *et al.* Identification of a core TP53 transcriptional program with highly distributed
475 tumor suppressive activity. *Genome Res* **27**, 1645-1657, doi:10.1101/gr.220533.117 (2017).
476 27 Sammons, M. A., Zhu, J., Drake, A. M. & Berger, S. L. TP53 engagement with the genome
477 occurs in distinct local chromatin environments via pioneer factor activity. *Genome Res* **25**, 179-
478 188, doi:10.1101/gr.181883.114 (2015).
479 28 Stark, C. *et al.* BioGRID: a general repository for interaction datasets. *Nucleic Acids Res* **34**,
480 D535-539, doi:10.1093/nar/gkj109 (2006).
481 29 Thul, P. J. *et al.* A subcellular map of the human proteome. *Science* **356**,
482 doi:10.1126/science.aal3321 (2017).
483 30 Badertscher, L. *et al.* Genome-wide RNAi Screening Identifies Protein Modules Required for
484 40S Subunit Synthesis in Human Cells. *Cell Rep* **13**, 2879-2891,
485 doi:10.1016/j.celrep.2015.11.061 (2015).
486 31 Zhang, S., Feng, Y., Narayan, O. & Zhao, L. J. Cytoplasmic retention of HIV-1 regulatory
487 protein Vpr by protein-protein interaction with a novel human cytoplasmic protein VprBP. *Gene*
488 **263**, 131-140, doi:10.1016/s0378-1119(00)00583-7 (2001).
489 32 Belzile, J. P., Abrahamyan, L. G., Gerard, F. C., Rougeau, N. & Cohen, E. A. Formation of
490 mobile chromatin-associated nuclear foci containing HIV-1 Vpr and VPRBP is critical for the
491 induction of G2 cell cycle arrest. *PLoS Pathog* **6**, e1001080, doi:10.1371/journal.ppat.1001080
492 (2010).
493 33 Yang, K., Yang, J. & Yi, J. Nucleolar Stress: hallmarks, sensing mechanism and diseases. *Cell*
494 *Stress* **2**, 125-140, doi:10.15698/cst2018.06.139 (2018).
495 34 Li, Y., Hu, Y., Che, L., Jia, J. & Chen, M. Nucleolar localization of Small G protein RhoA is
496 associated with active RNA synthesis in human carcinoma HEp-2 cells. *Oncol Lett* **11**, 3605-
497 3610, doi:10.3892/ol.2016.4450 (2016).

498 35 Hattab, E. M., Koch, M. O., Eble, J. N., Lin, H. & Cheng, L. Tertiary Gleason pattern 5 is a
499 powerful predictor of biochemical relapse in patients with Gleason score 7 prostatic
500 adenocarcinoma. *J Urol* **175**, 1695-1699; discussion 1699, doi:10.1016/S0022-5347(05)00998-5
501 (2006).
502 36 Nelson, P. S. *et al.* The program of androgen-responsive genes in neoplastic prostate epithelium.
503 *Proc Natl Acad Sci U S A* **99**, 11890-11895, doi:10.1073/pnas.182376299 (2002).
504 37 Takayama, K. *et al.* Identification of novel androgen response genes in prostate cancer cells by
505 coupling chromatin immunoprecipitation and genomic microarray analysis. *Oncogene* **26**, 4453-
506 4463, doi:10.1038/sj.onc.1210229 (2007).
507 38 Wang, G., Jones, S. J., Marra, M. A. & Sadar, M. D. Identification of genes targeted by the
508 androgen and PKA signaling pathways in prostate cancer cells. *Oncogene* **25**, 7311-7323,
509 doi:10.1038/sj.onc.1209715 (2006).
510 39 Liberzon, A. *et al.* Molecular signatures database (MSigDB) 3.0. *Bioinformatics* **27**, 1739-1740,
511 doi:10.1093/bioinformatics/btr260 (2011).
512 40 Schubert, M. *et al.* Perturbation-response genes reveal signaling footprints in cancer gene
513 expression. *Nat Commun* **9**, 20, doi:10.1038/s41467-017-02391-6 (2018).
514 41 Le Rouzic, E. *et al.* HIV1 Vpr arrests the cell cycle by recruiting DCAF1/VprBP, a receptor of
515 the Cul4-DDB1 ubiquitin ligase. *Cell Cycle* **6**, 182-188, doi:10.4161/cc.6.2.3732 (2007).
516 42 Hrecka, K. *et al.* Lentiviral Vpr usurps Cul4-DDB1[VprBP] E3 ubiquitin ligase to modulate cell
517 cycle. *Proc Natl Acad Sci U S A* **104**, 11778-11783, doi:10.1073/pnas.0702102104 (2007).
518 43 Swamy, M. *et al.* Glucose and glutamine fuel protein O-GlcNAcylation to control T cell self-
519 renewal and malignancy. *Nat Immunol* **17**, 712-720, doi:10.1038/ni.3439 (2016).
520 44 Kim, K. *et al.* Vpr-binding protein antagonizes p53-mediated transcription via direct interaction
521 with H3 tail. *Mol Cell Biol* **32**, 783-796, doi:10.1128/MCB.06037-11 (2012).
522 45 Sollinger, H. W. Mycophenolate mofetil. *Kidney Int Suppl* **52**, S14-17 (1995).
523

524 **Figure legends**

525 1. Identification of VPRBP as an AR and O-GlcNAc co-regulated target. (A) Venn diagrams showing the
526 distribution of peaks in relation to genes in AR and O-GlcNAc consensus ChIP-seq, generated using
527 CEAS tool in galaxy cistrome. (B) ChIP-seq enrichment of AR and O-GlcNAc at VPRBP promoter region
528 using UCSC genome browser. (C) Percentage recovery of CAMKK2 and VPRBP with AR ChIP; and
529 PPAT/PAICS and VPRBP with O-GlcNAc ChIP in vehicle (0.01% ethanol) and 1nM R1881 4h and 24h
530 treated LNCaP cells. (D) mRNA expression of VPRBP, CAMKK2 and UAP1 in LNCaP treated with
531 vehicle or 1nM R1881 for 24 h was detected by qRT-PCR. Results are normalized to RPLPO as
532 housekeeping control. (E) Time dependency of VPRBP expression following exposure to 1nM R1881 for

533 different time points. LNCaP cells were androgen deprived for 3 days prior to stimulation with vehicle or
534 1 nM R1881. p values by Student's t test. ** =p < 0.01; *** = p < 0.001.
535 2. OGT is required for VPRBP stability. (A) LNCaP cells were transiently transfected with OGT siRNA
536 and cells were harvested 5d post transfection to detect mRNA expression of VPRBP, OGT and OGA by
537 qRT-PCR and (B) protein expression by immunoblot analysis under basal conditions. (C) For detection
538 of protein expression under androgen stimulated conditions, LNCaP cells were transfected with OGT
539 siRNAs or scrambled siRNA (scr si) followed by androgen deprivation for 72 h prior to 1nM R1881
540 stimulation for 24h. (D) The O-GlcNAcylation of immunoprecipitated (IP) VPRBP from LNCaP cells
541 was detected by immunoblotting (IB) with RL2 antibody. (E) The effect of OGT inhibitors 40 μM OSMI2
542 and 10 μM OSMI3 on VPRBP protein levels following 24h treatment was detected by immnuoblot
543 analysis. Results are expressed as means ± SD from at least three independent experiments. *** = p <
544 0.001 by Student's t test.
545 3. VPRBP knockdown leads to reduced cell proliferation and p53 stabilization. (A) LNCaP cells were
546 transfected with VPRBP siRNA and cells were harvested 3d post transfection to detect mRNA expression
547 of VPRBP, OGT, p53 and p21. (B) Effect of VPRBP knockdown on LNCaP cell proliferation was
548 assessed by cell counting 5d post transfection; the cells were grown in the presence (CM) and absence of
549 androgens (ADM). (C) Effect of VPRBP knockdown on LNCaP p53, markers of cell cycle and other
550 proteins of interest was assessed by immunoblot analysis of cell lysate prepared 3d post transfection. (D)
551 Effect of VPRBP knockdown on cell proliferation was assessed by cell counting 5d post transfection in
552 VCaP cells grown in the presence (CM) and absence of androgens (ADM). (E) Effect of VPRBP
553 knockdown on VCaP proteins of interest was assessed by immunoblot analysis. Results are expressed as
554 means ± SD. * =p < 0.05, ** =p < 0.01; *** = p < 0.00. Statistical analyses were performed by Student's
555 t test for qPCR and one-way ANOVA followed by Tukey's posthoc analysis for cell proliferation.

556 4. VPRBP knockdown increases p53 chromatin recruitment and induces nucleolar stress. (A) Bar graph
557 showing percentage recovery of p21 and negative site primer (CCND1) following p53 ChIP in different
558 transfection conditions. (B) Table showing the number of peaks obtained under different conditions. (C)
559 Venn diagram showing the overlap of our nutlin-3a p53 ChIP-seq in LNCaP cells with previously reported
560 nutlin-3a p53 ChIP-seq in MCF7 cells (GSE86164). (D) Venn diagram showing the overlap of nutlin-3a
561 p53 ChIP-seq in LNCaP with VPRBPsi p53 ChIP-seq consensus sites. (E) Venn diagram showing the
562 overlap of VPRBPsi p53 ChIP-seq consensus sites with previously reported nutlin-3a p53 ChIP-seq in
563 MCF7 cells. (F) Venn diagram showing the overlap of VPRBP interactome with nucleolar proteome. (G)
564 Representative immunofluorescence images showing VPRBP and fibrillarin staining in scrambled and
565 VPRBP siRNA transfected LNCaPs 3d post transfection (scale bar= 10μm).
566 5. VPRBP protein expression correlates with AR amplification, OGT overexpression and poor prognosis.
567 Bar graphs showing positive correlation of VPRBP expression with AR (A) and OGT expression (B) by
568 IHC in TMA sections. (C) PSA recurrence free survival curves in patients expressing low or high levels
569 of AR where VPRBP expression was present or absent and (D) survival curves in patients expressing no,
570 low or high levels of OGT where VPRBP expression was present or absent. (E) Scatter plot comparing
571 AR mRNA expression to VRPBP mRNA expression in TCGA PanCancer Atlas prostate dataset. (F) Box
572 plot showing association between VPRBP expression quartiles and the 139 up-regulated AR genes from
573 heat map. (G) Scatter plot comparing GSEA Hallmark "P53 Pathway" to VRPBP mRNA expression in
574 TCGA PanCancer Atlas prostate dataset. (H) Scatter plots showing VPRBP expression in Taylor data sets
575 versus p53 progeny scores.
576 6. Model depicting VPRBP regulation in prostate cancer. AR activation by androgens (A) stimulate
577 *VPRBP* gene expression in the presence of hitherto unknown O-GlcNAcylated TF/s. VPRBP protein is
578 further stabilized by OGT whereas VPRBP diminishes p53 stability and vice versa. VPRBP also

579 suppresses p53 recruitment to the chromatin thereby regulating p53 activation and inducing cell
580 proliferation and tumor growth.

581 **Supplementary figures**

582 S1.VPRBP is a novel AR target (A) Bar graphs showing relative enrichments in CAMKK2 and VPRBP
583 with AR ChIP-qPCR in vehicle vs R1881 (24h) treated LNCaP cells; and relative enrichments in
584 PPAT/PAICS and VPRBP with O-GlcNAc ChIP. (B) Graphs showing quantitation of western bands of
585 Figure 1E done using image J software and normalized to β-actin. (C) qRT-PCR analysis of VPRBP,
586 CAMKK2 and UAP1 expression in LNCaP cells treated with vehicle (0.01% ethanol) or 1nM DHT for
587 24h following androgen deprivation for 72h. (D) Western blot analysis of LNCaP cells treated with vehicle
588 or DHT (1nM and 10nM) for 24 h. Results are expressed as means ± SD. * =$p < 0.05$, ** =$p < 0.01$; ***
589 = $p < 0.001$ by Student's t test.

590 S2. OGT is required for VPRBP stability. (A) Graphs showing quantitation of western bands (Fig. 2B)
591 from OGT siRNA transfected cells vs scrambled control using image J software and normalized to β-
592 actin. (B) Graphs showing quantitation of western bands (Fig. 2E) from OSMI2/OSMI3 treatments and
593 normalized to β-actin. (C) qRT-PCR analysis VPRBP and OGT expression in LNCaP cells treated with
594 vehicle or 40 μM OSMI2 or 10 μM OSMI3 for 24h with RPLPO as internal control. Results are expressed
595 as means ± SD. * =$p < 0.05$, ** =$p < 0.01$; *** = $p < 0.001$ by Student's t test.

596 S3. (A) Effect of VPRBP kinase activity inhibitor, B32B3 on LNCaP cell proliferation was assessed by
597 cell counting 4d post treatment in the presence and absence of OSMI2 and OSMI3. (B) Graphs showing
598 quantitation of western bands (Fig. 3C) from VPRBP siRNA transfected cells *vs* scrambled control using
599 image J software and normalized to β-actin. Results are expressed as means ± SD. * =$p < 0.05$, ** =$p <$
600 0.01; *** = $p < 0.001$ by Student's t test.

601 S4. VPRBP and p53 exhibit reciprocal relation. (A) Western image showing time dependent reduction in
602 p53 expression following exposure to 1nM R1881 for different time points. (B) qRT-PCR analysis of p53
603 expression in LNCaP cells treated with vehicle or 1nM R1881 for 24h with RPLPO as internal control.
604 (C) Bar graphs showing relative enrichments in p21 with p53 ChIP-qPCR in vehicle and R1881 24h
605 treated LNCaP cells. (D) Bar graphs showing percentage recovery of p21, VPRBP and negative primers
606 with p53 ChIP-qPCR in vehicle (DMSO) and nutlin-3a 24h treated LNCaP. (E) ChIP-seq enrichment
607 profile of nutlin-3a p53 ChIP-seq at CDKN1A (p21) promoter region (top) and absence of enrichment at
608 VPRBP promoter region (bottom), using UCSC genome browser. (F) Protein expression of VPRBP, p53
609 and p21 by immunoblot analysis following vehicle and nutlin-3a treatment for 24h; and wild type versus
610 p53 knockout LNCaP cells, and (G) mRNA expression by qRT-PCR. Results are expressed as means ±
611 SD. *** = $p < 0.001$ by Student's t test.
612 S5. (A) Venn diagram showing the overlap of our nutlin-3a p53 ChIP-seq in LNCaP with previously
613 reported nutlin-3a p53 ChIP-seq in HCT116 (GSE86164), Bone/SJSA (GSE86164) and IMR90 fetal lung
614 fibroblasts (GSE58740). (B) Venn diagram showing the overlap of VPRBP si1 and VPRBP si2 p53 ChIP-
615 seq peaks; overlap of OGT si1 and OGT si2 p53 ChIP seq peaks; and overlap of scr, VPRBPsi and OGTsi
616 ChIP-seq peaks. (C) CEAS analysis of VPRBP si p53 ChIP-seq in LNCaP. (E) Venn diagram showing
617 overlap of VPRBP si p53 ChIP-seq with H3K27Ac ChIP-seq and H3K27me3 ChIP-seq in ethanol treated
618 LNCaP-MYC cells (GSE73994) (F).Table showing the top over-represented motifs obtained from motif
619 enrichment analysis of VPRBP si p53 ChIP-seq using P-scan ChIP.
620 S6. (A) Effect of VPRBP knockdown on fibrillarin, RPS8 and RPL5 was assessed by immunoblot analysis
621 and (B) graphs showing quantitation of the western bands. (C) IHC representative images showing
622 negative, weak, moderate and strong staining of VPRBP. (D) Survival curve showing inverse relation

623 between VPRBP expression and PSA recurrence free survival. Results of western quantitation are
624 expressed as means ± SD. * =p< 0.05 by Student's t test.
625 S7. Heatmaps comparing the expression of a total of 467 AR activity gene signatures combined from
626 multiple studies, in high and low VPRBP quartiles, created using the R package.
627

Figure 1

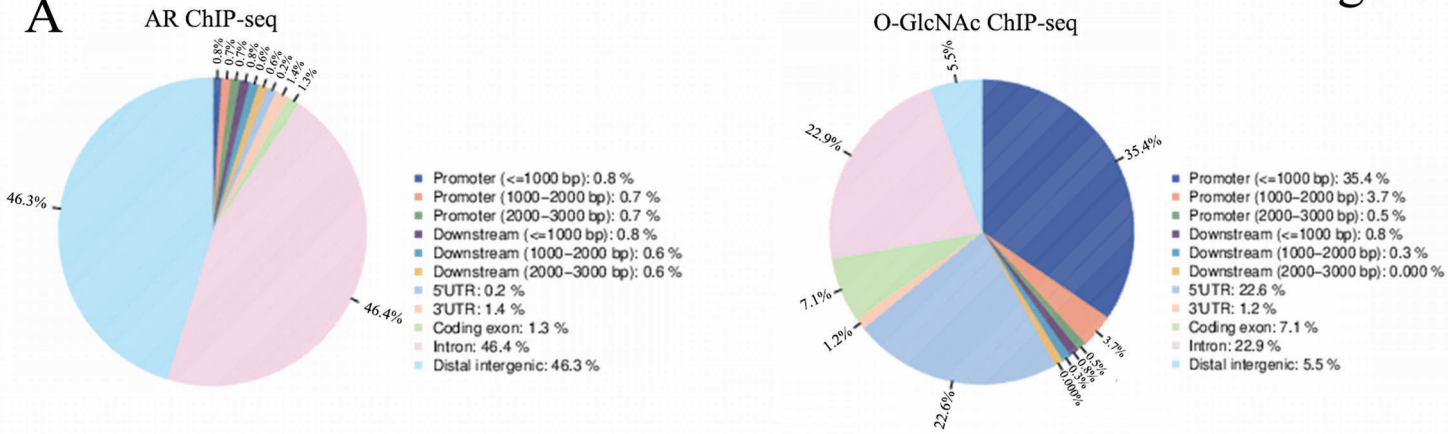
A
AR ChIP-seq
46.3%
46.4%
Promoter (<=1000 bp): 0.8 %
Promoter (1000–2000 bp): 0.7 %
Promoter (2000–3000 bp): 0.7 %
Downstream (<=1000 bp): 0.8 %
Downstream (1000–2000 bp): 0.6 %
Downstream (2000–3000 bp): 0.6 %
5'UTR: 0.2 %
3'UTR: 1.4 %
Coding exon: 1.3 %
Intron: 46.4 %
Distal intergenic: 46.3 %
O-GlcNAc ChIP-seq
5.5%
22.9%
35.4%
7.1%
1.2%
3.7%
22.6%
Promoter (<=1000 bp): 35.4 %
Promoter (1000–2000 bp): 3.7 %
Promoter (2000–3000 bp): 0.5 %
Downstream (<=1000 bp): 0.8 %
Downstream (1000–2000 bp): 0.3 %
Downstream (2000–3000 bp): 0.000 %
5'UTR: 22.6 %
3'UTR: 1.2 %
Coding exon: 7.1 %
Intron: 22.9 %
Distal intergenic: 5.5 %

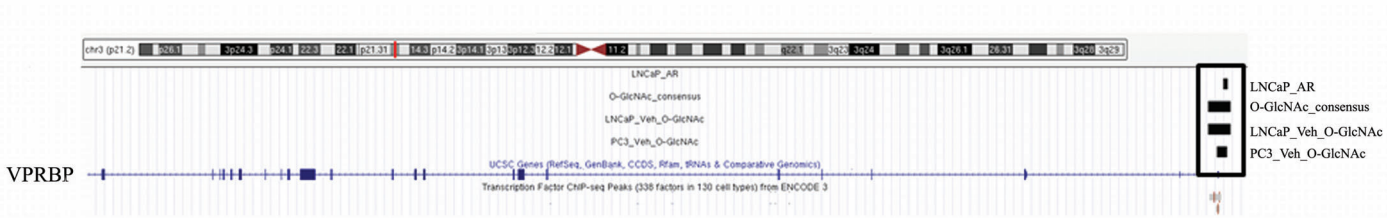
B
LNCaP_AR
O-GlcNAc_consensus
LNCaP_Veh_O-GlcNAc
PC3_Veh_O-GlcNAc
VPRBP
UCSC Genes (RefSeq, GenBank, CCDS, Rfam, tRNAs & Comparative Genomics)
Transcription Factor ChIP-seq Peaks (338 factors in 130 cell types) from ENCODE 3

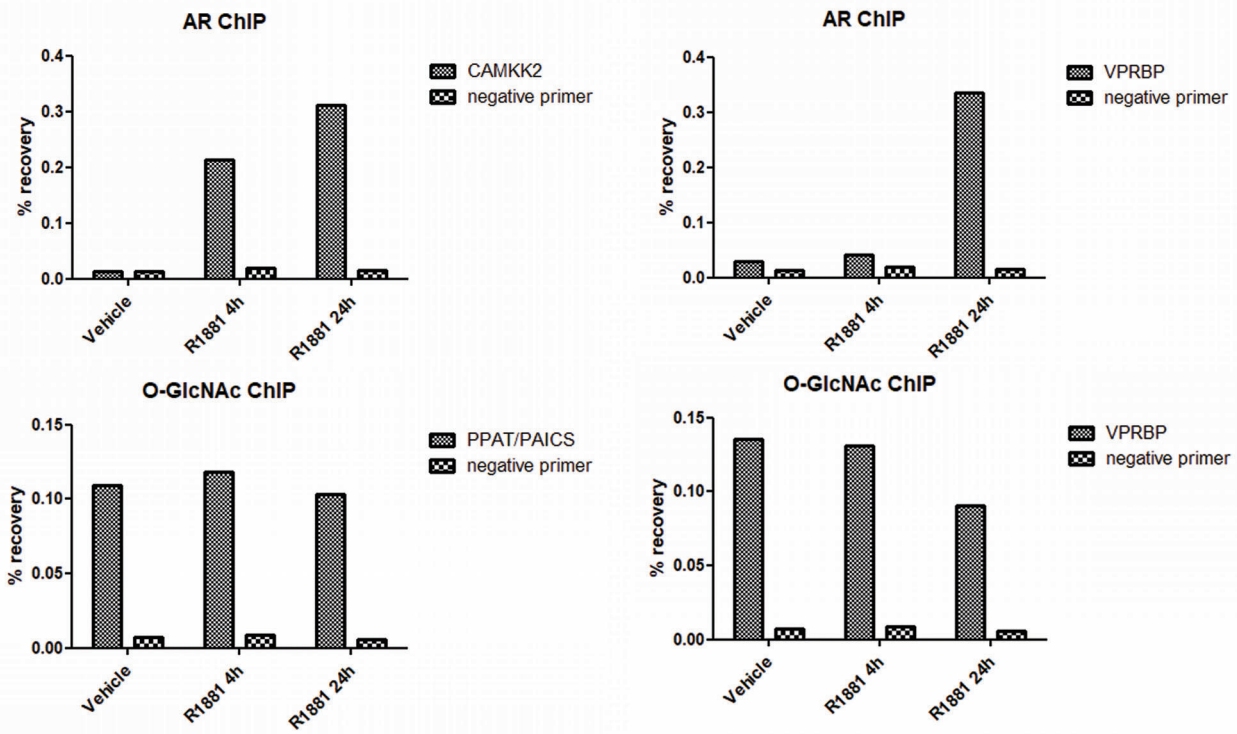
C
AR ChIP
% recovery
CAMKK2
negative primer
Vehicle
R1881 4h
R1881 24h
AR ChIP
VPRBP
negative primer
O-GlcNAc ChIP
PPAT/PAICS
negative primer
O-GlcNAc ChIP
VPRBP
negative primer

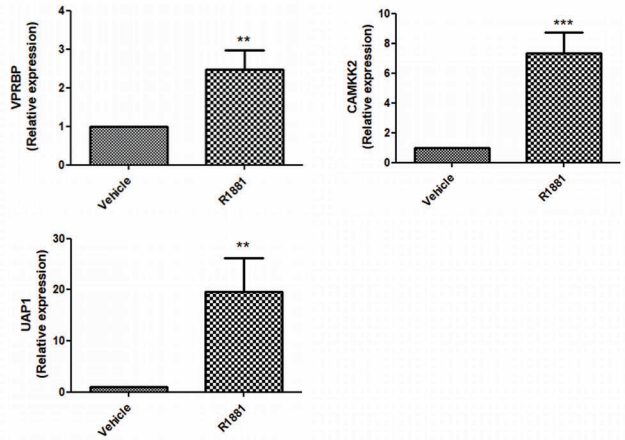
D
VPRBP (Relative expression)
CAMKK2 (Relative expression)
UAP1 (Relative expression)
Vehicle
R1881

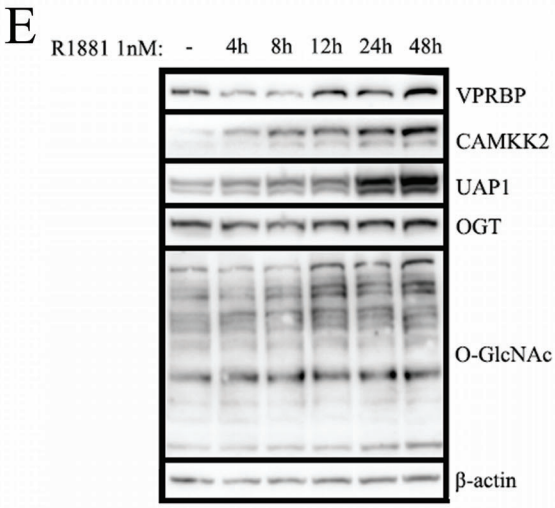
E
R1881 1nM: - 4h 8h 12h 24h 48h
VPRBP
CAMKK2
UAP1
OGT
O-GlcNAc
β-actin

Figure 2

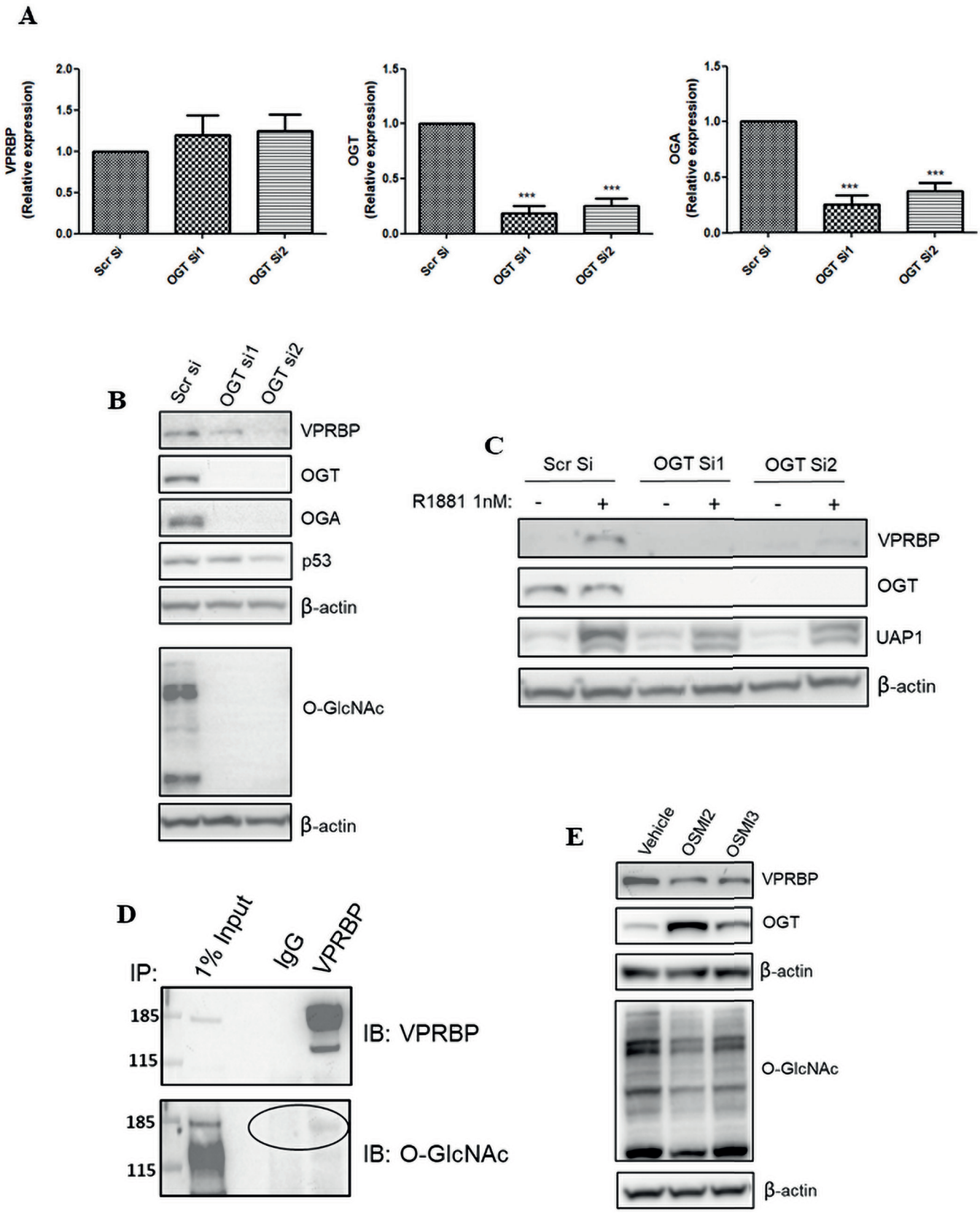
A
VPRBP (Relative expression)
OGT (Relative expression)
OGA (Relative expression)
Scr Si
OGT Si1
OGT Si2
***
B
Scr si
OGT si1
OGT si2
VPRBP
OGT
OGA
p53
β-actin
O-GlcNAc
β-actin
C
Scr Si
OGT Si1
OGT Si2
R1881 1nM:
-
+
VPRBP
OGT
UAP1
β-actin
D
IP:
1% Input
IgG
VPRBP
185
115
IB: VPRBP
IB: O-GlcNAc
E
Vehicle
OSMI2
OSMI3
VPRBP
OGT
β-actin
O-GlcNAc
β-actin

Figure 3

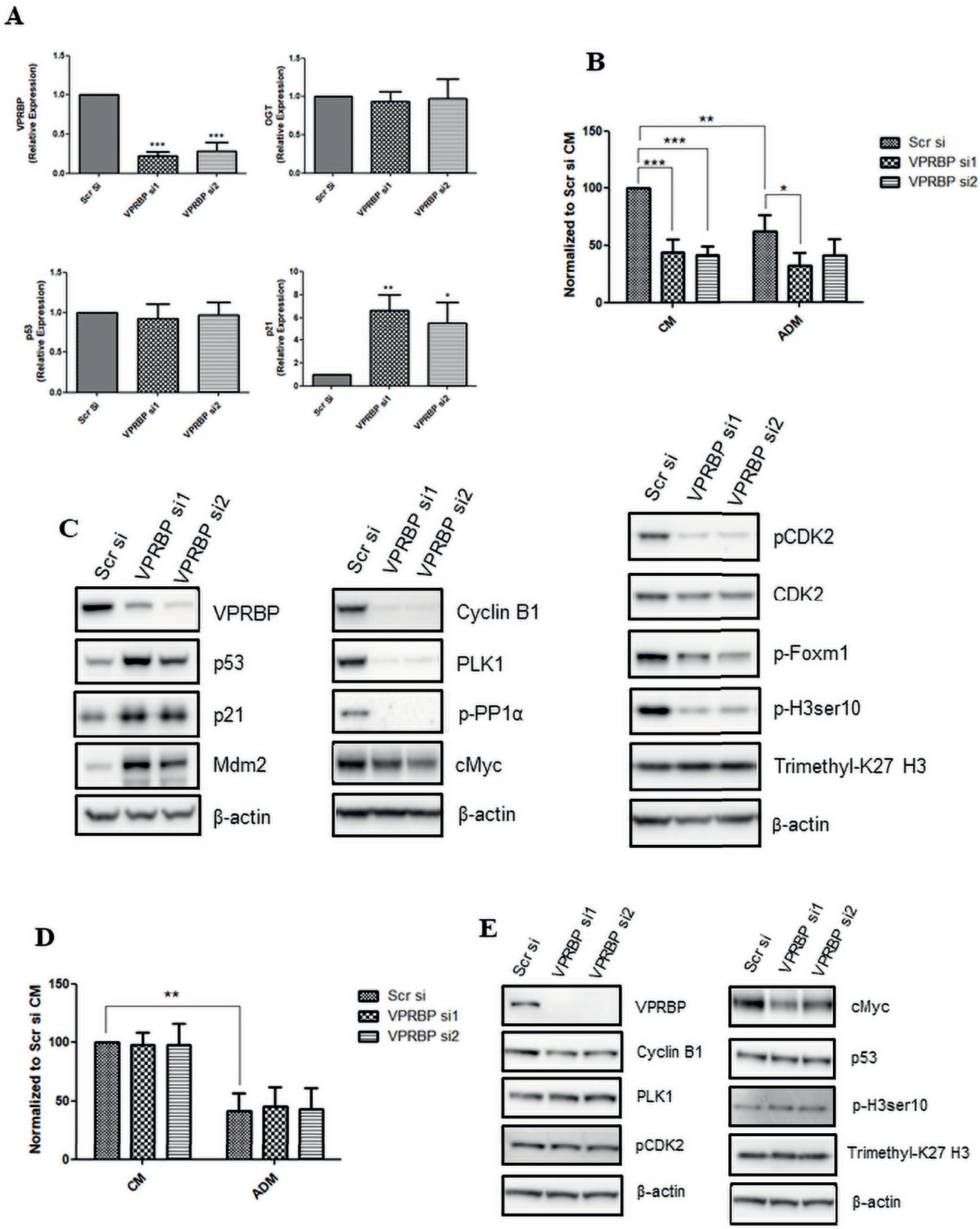
A
VPRBP (Relative Expression)
OGT (Relative Expression)
p53 (Relative Expression)
p21 (Relative Expression)
Scr si
VPRBP si1
VPRBP si2
B
Normalized to Scr si CM
CM
ADM
C
VPRBP
p53
p21
Mdm2
β-actin
Cyclin B1
PLK1
p-PP1α
cMyc
pCDK2
CDK2
p-Foxm1
p-H3ser10
Trimethyl-K27 H3
D
E

Figure 4

A

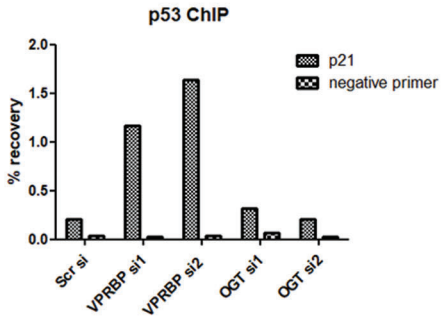

B

ChIP conditions	Number of peaks
LNCaP_VPRBP_Si1_p53	2326
LNCaP_VPRBP_Si2_p53	1639
LNCaP_Nutlin_3A_p53	582
LNCaP_OGT_Si1_p53	412
LNCaP_OGT_Si1_p53	423
LNCaP_Scr_Si_p53	425

C

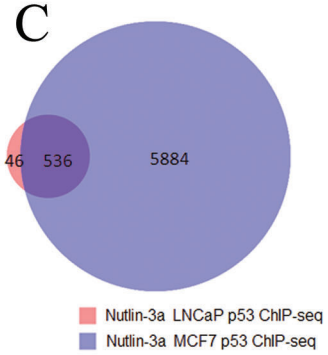

D

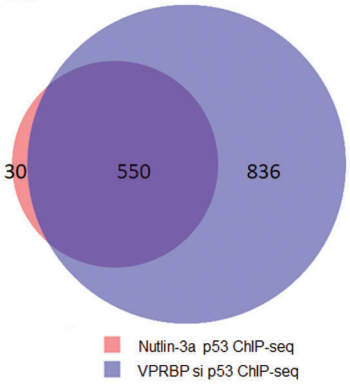

E

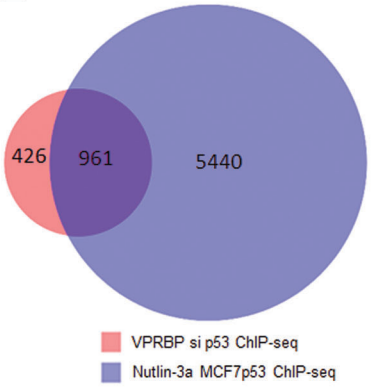

F

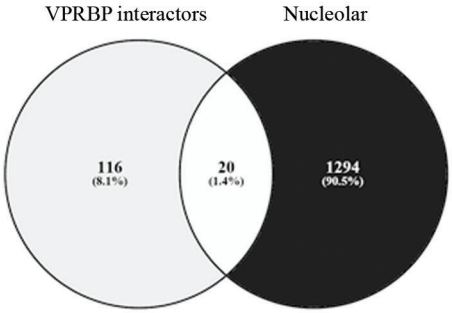

G

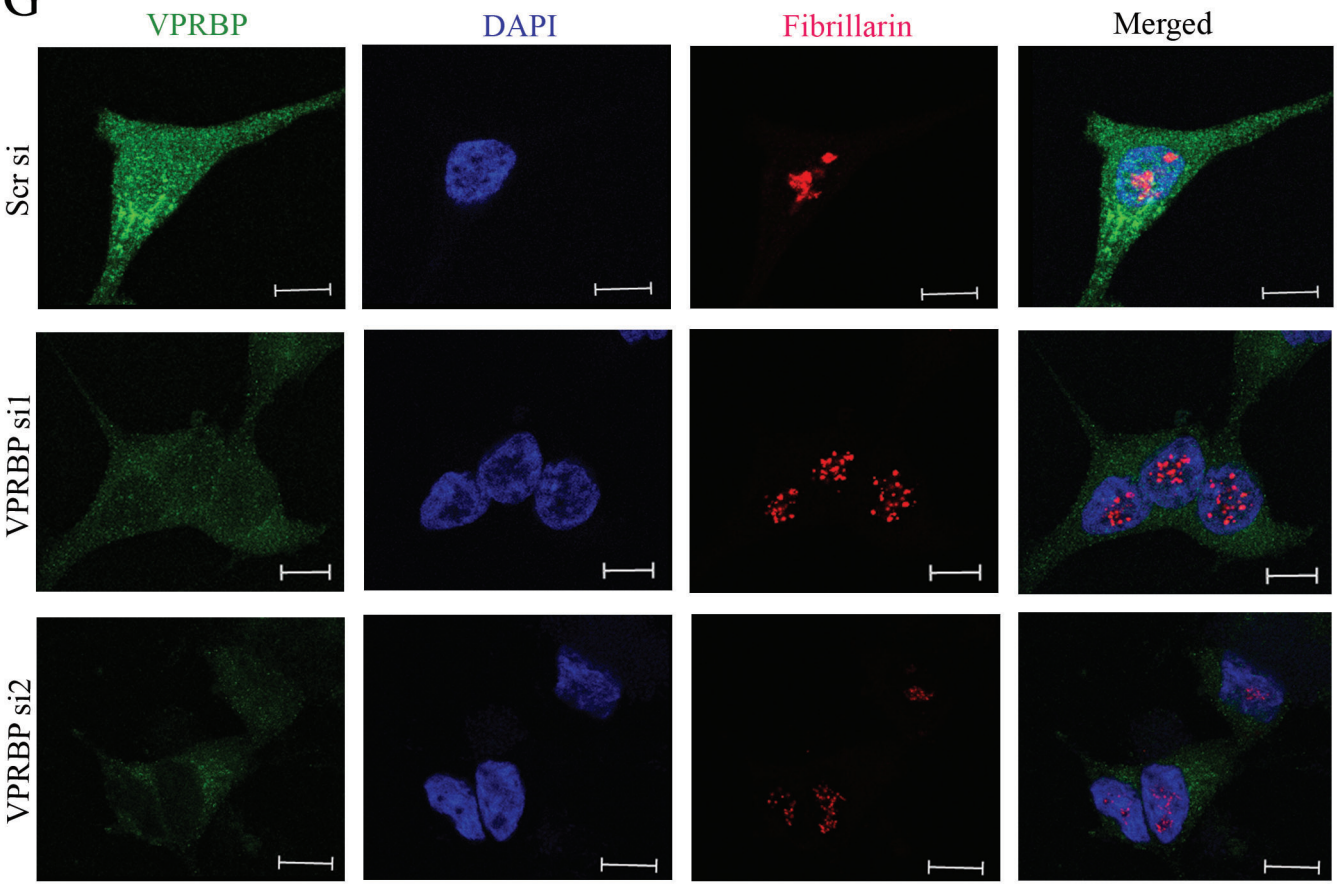

Figure 5

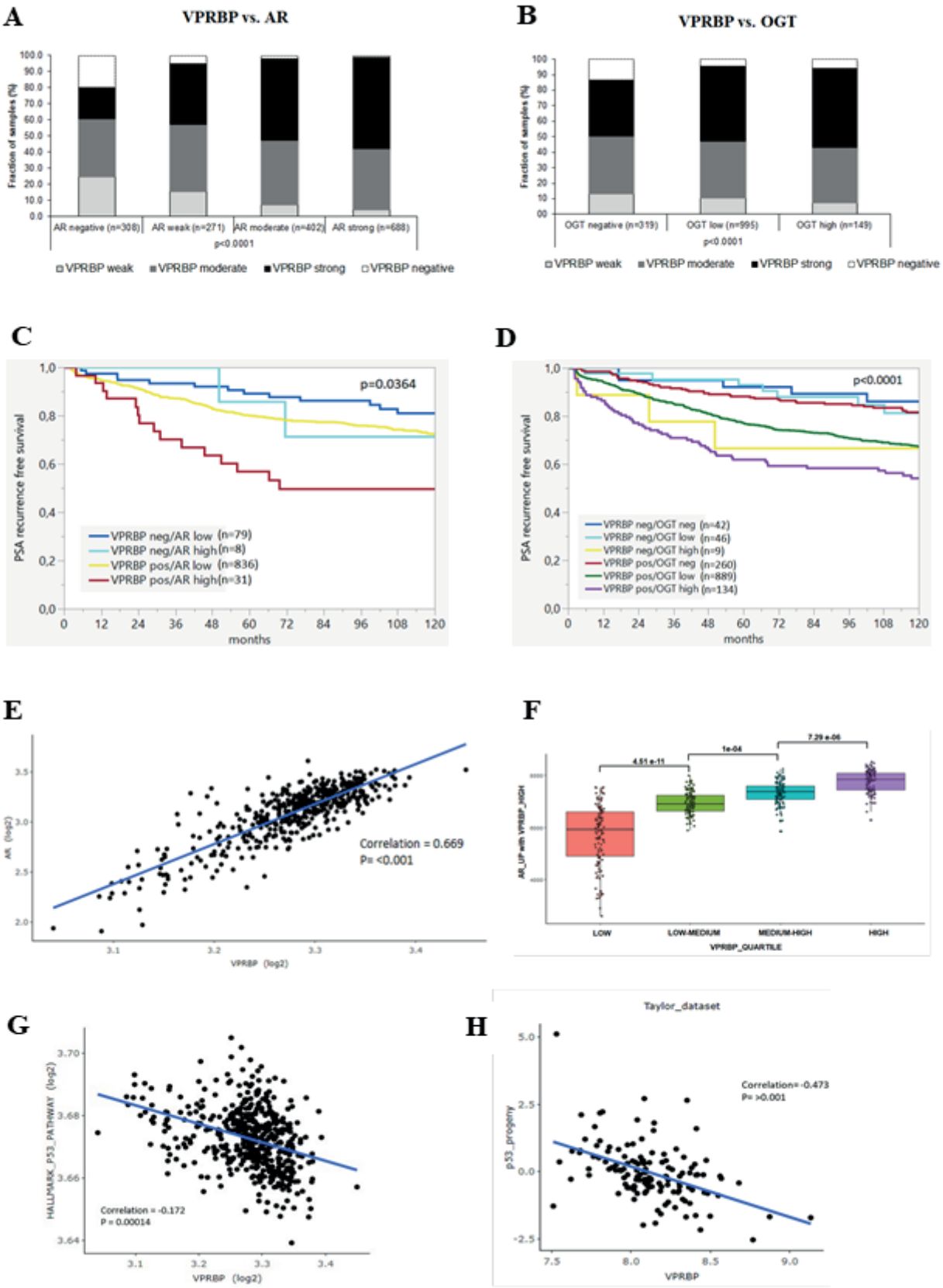
A
VPRBP vs. AR
Fraction of samples (%)
AR negative (n=308)
AR weak (n=271)
AR moderate (n=402)
AR strong (n=688)
p<0.0001
VPRBP weak
VPRBP moderate
VPRBP strong
VPRBP negative
B
VPRBP vs. OGT
Fraction of samples (%)
OGT negative (n=319)
OGT low (n=995)
OGT high (n=149)
p<0.0001
VPRBP weak
VPRBP moderate
VPRBP strong
VPRBP negative
C
p=0.0364
PSA recurrence free survival
VPRBP neg/AR low (n=79)
VPRBP neg/AR high (n=8)
VPRBP pos/AR low (n=836)
VPRBP pos/AR high (n=31)
months
D
p<0.0001
PSA recurrence free survival
VPRBP neg/OGT neg (n=42)
VPRBP neg/OGT low (n=46)
VPRBP neg/OGT high (n=9)
VPRBP pos/OGT neg (n=260)
VPRBP pos/OGT low (n=889)
VPRBP pos/OGT high (n=134)
months
E
AR (log2)
Correlation = 0.669
P= <0.001
VPRBP (log2)
F
4.51 e-11
1e-04
7.29 e-06
AR_UP with VPRBP_HIGH
LOW
LOW-MEDIUM
MEDIUM-HIGH
HIGH
VPRBP_QUARTILE
G
HALLMARK_P53_PATHWAY (log2)
Correlation = -0.172
P = 0.00014
VPRBP (log2)
H
Taylor_dataset
p53_progeny
Correlation= -0.473
P= >0.001
VPRBP

Figure 6

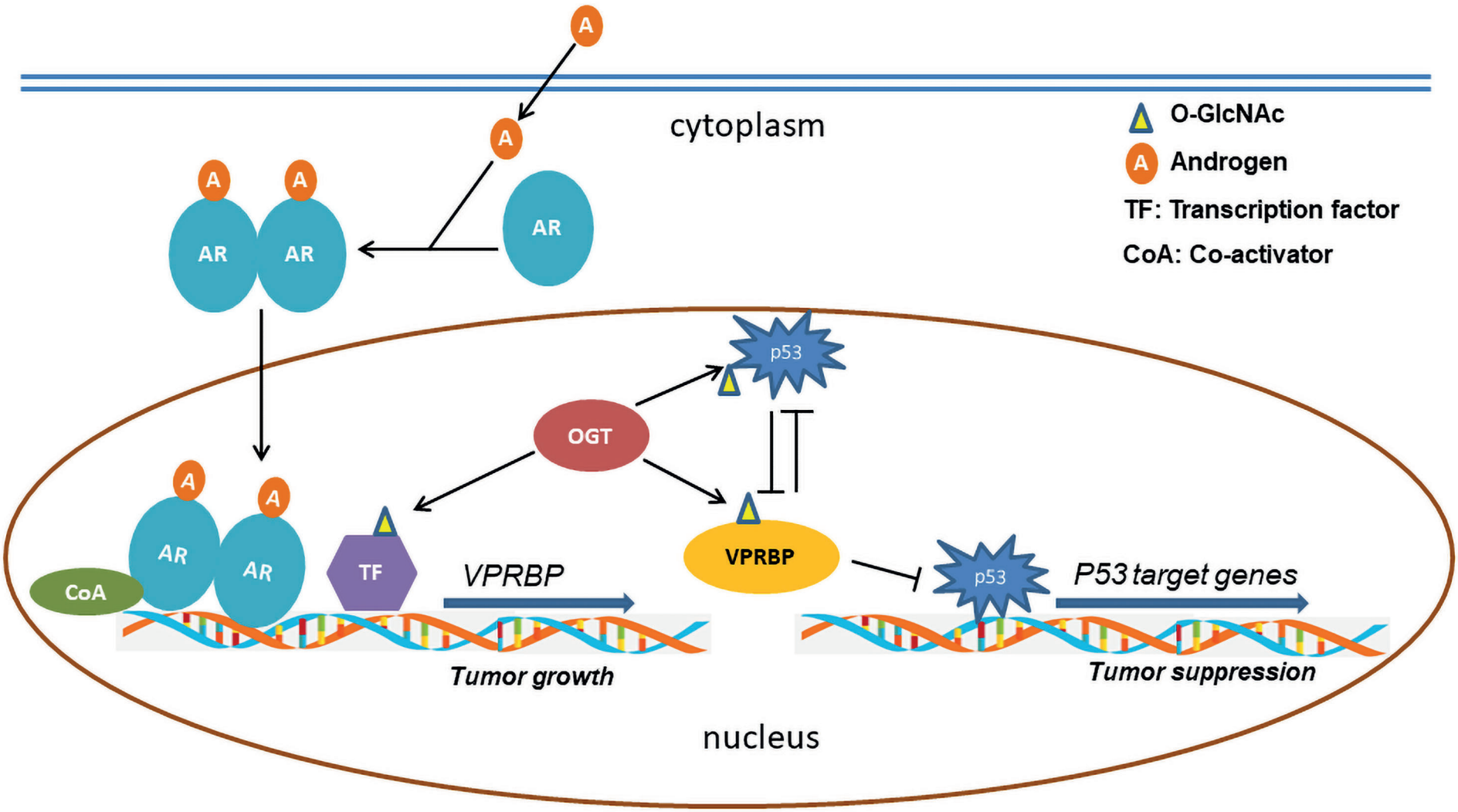
A
A
cytoplasm
O-GlcNAc
A Androgen
TF: Transcription factor
CoA: Co-activator
A
A
AR
AR
AR
p53
OGT
A
A
AR
AR
CoA
TF
VPRBP
VPRBP
p53
P53 target genes
Tumor growth
Tumor suppression
nucleus

Supplementary Figure S1

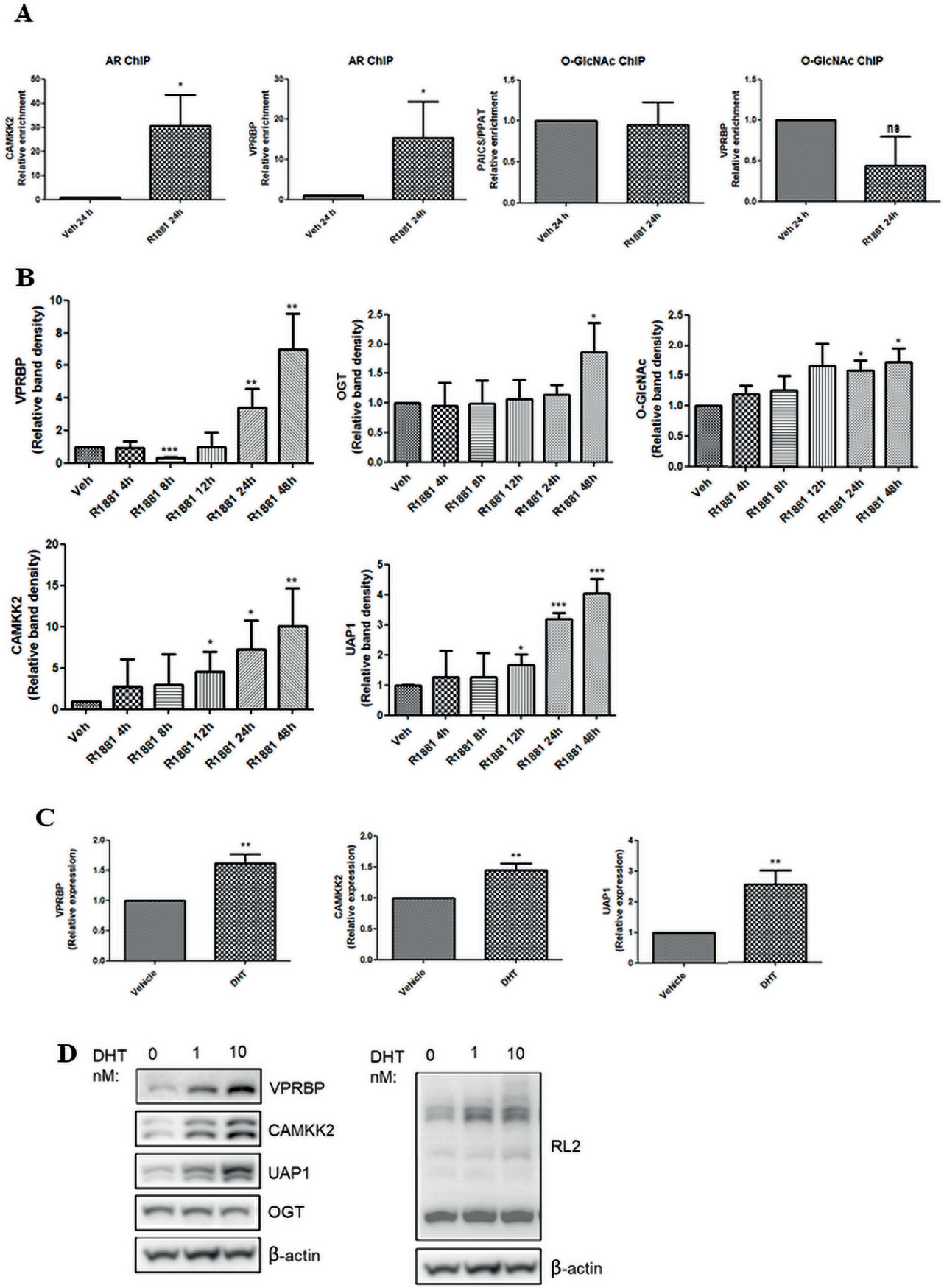

Supplementary Figure S2

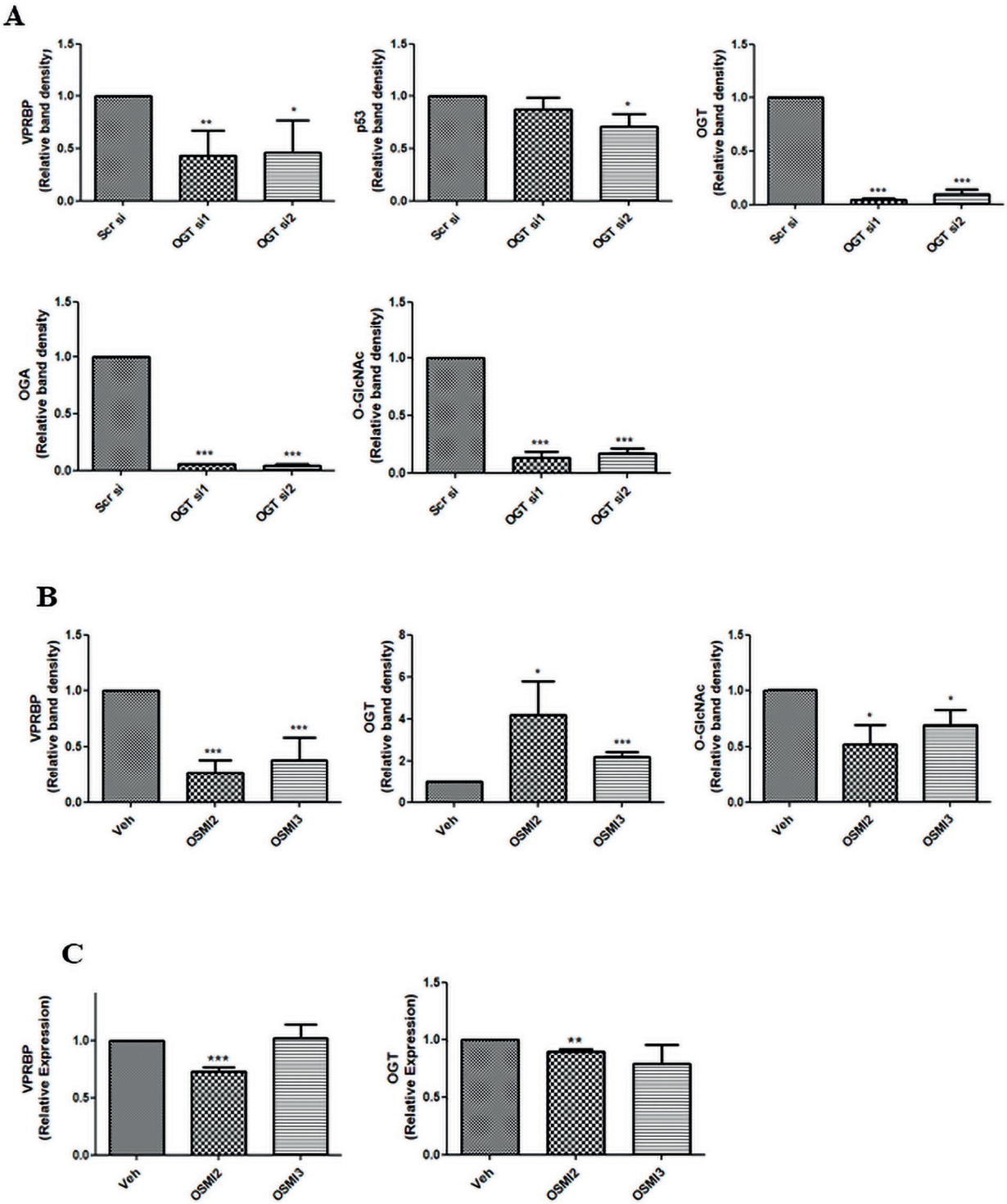

Supplementary Figure S3

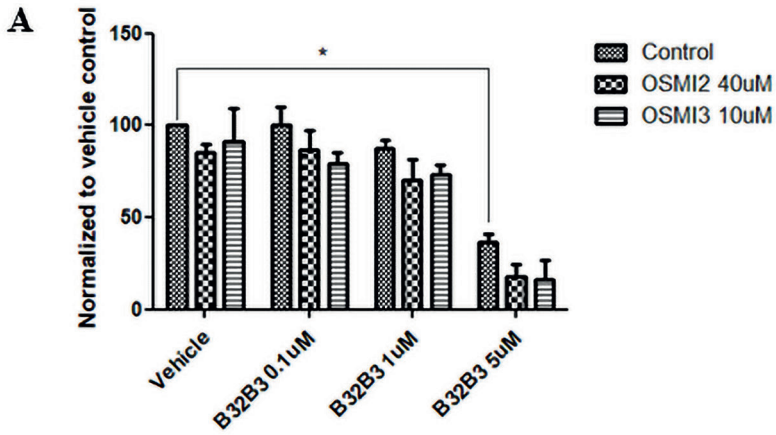

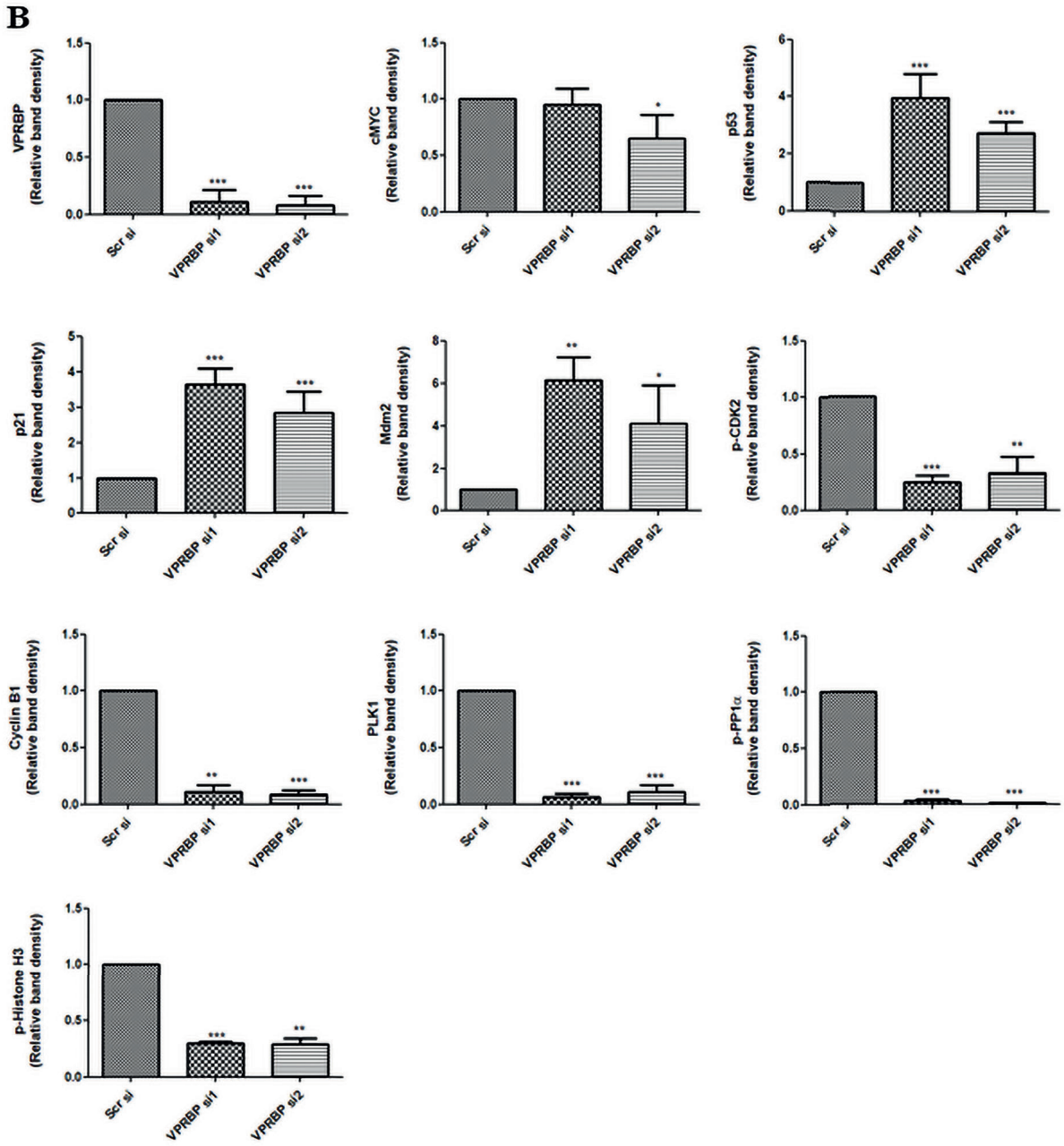

Supplementary Figure S4

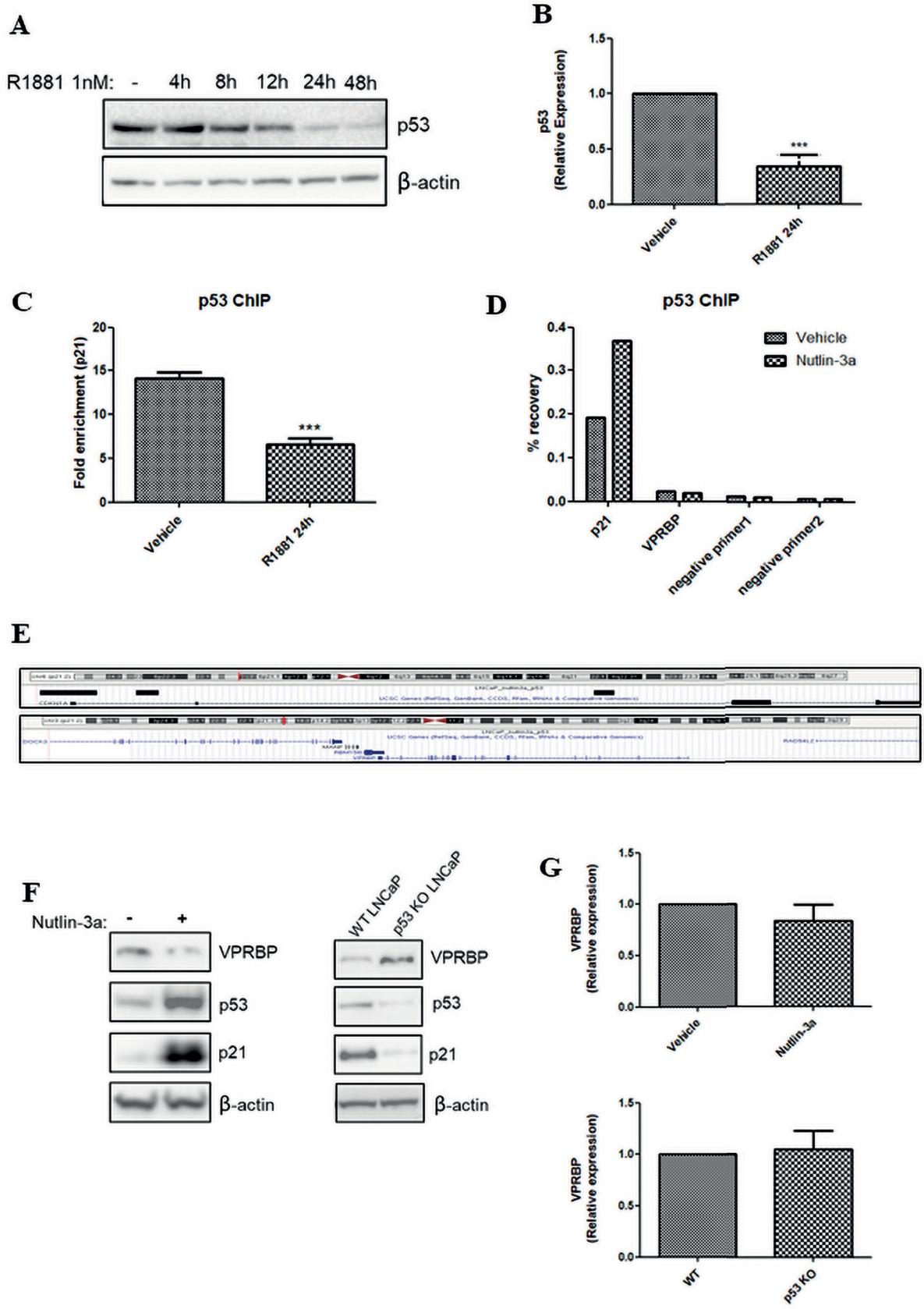

Supplementary Figure S5

A

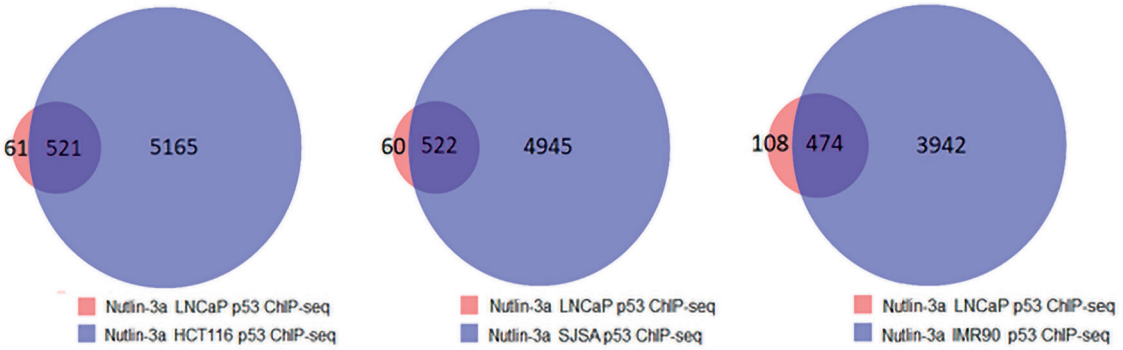

B

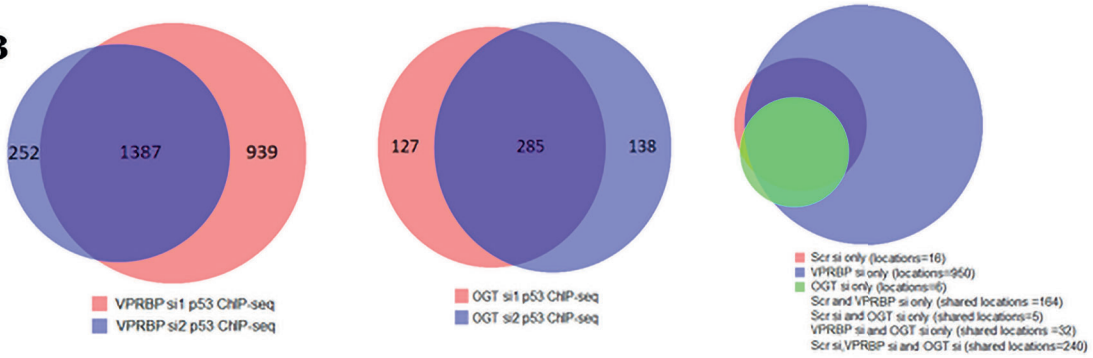

C VPRBP siLNCAP p53 ChIP-seq

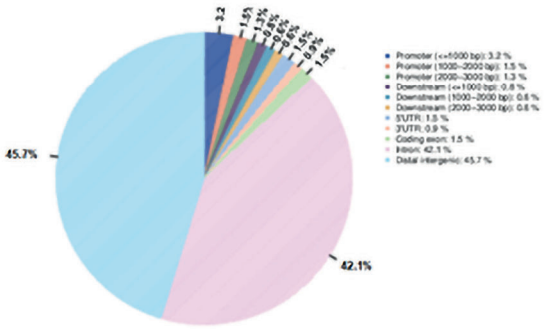

D

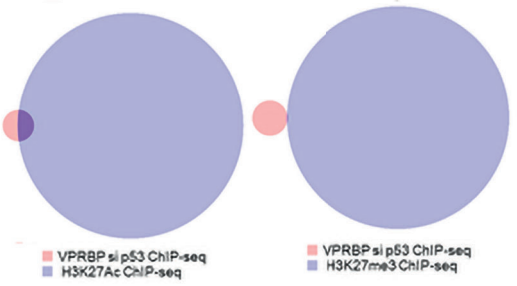

E

Name	ID	L.PV	L.O/U	G.PV	G.O/U	SP.COR	P.POS	P.POS.PV
TP53	MA0106.3	1.5E-274	↑	3.5E-271	↑	-0.085	[-6,4]	7.2E-19
TP73	MA0861.1	2.8E-264	↑	3.1E-254	↑	-0.0464	[-6,4]	3.7E-17
TP63	MA0525.2	3.5E-205	↑	2.8E-209	↑	-0.0242	[-6,4]	1.4E-16
SMAD3	MA0795.1	2.5E-55	↑	8.9E-72	↑	-0.0692	[-5,5]	0.3783
HES5	MA0821.1	1.6E-43	↑	6.0E-43	↑	0.0109	[-14,-4]	0.0016
HIF1A	MA1106.1	1.9E-37	↑	5.6E-43	↑	0.0343	[-10,0]	0.0002
HES7	MA0822.1	3.7E-33	↑	4.6E-29	↑	0.0019	[-14,-4]	0.0861
HIC2	MA0738.1	3.2E-32	↑	2.4E-39	↑	-0.0213	[-1,9]	1.1E-6
HEY2	MA0649.1	4.6E-30	↑	2.5E-33	↑	0.0281	[-10,0]	0.0072
CLOCK	MA0819.1	1.3E-28	↑	6.3E-24	↑	-0.0039	[-10,0]	8.6E-9
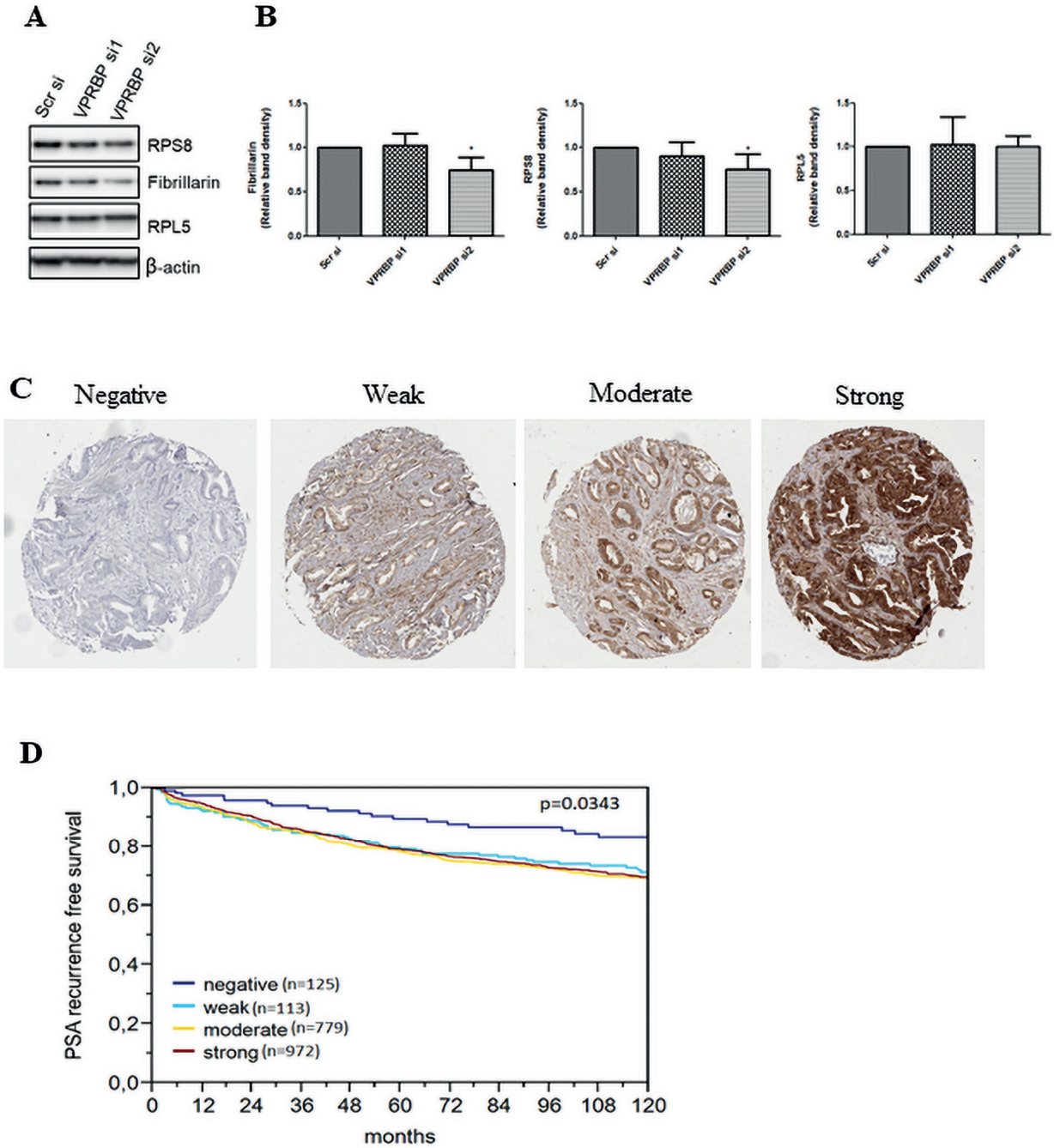
Supplementary Figure S6